A Dock-and-Lock Mechanism Clusters ADAM10 at Cell-Cell Junctions to Promote α-Toxin Cytotoxicity

Jimit Shah, Florian Rouaud, Diego Guerrera, Ekaterina Vasileva, Lauren M Popov, William L Kelley, Eric Rubinstein, Jan E Carette, Manuel R Amieva, Sandra Citi

HAL Id: inserm-03941903
https://inserm.hal.science/inserm-03941903

Submitted on 16 Jan 2023

Cell Reports

A Dock-and-Lock Mechanism Clusters ADAM10 at Cell-Cell Junctions to Promote α-Toxin Cytotoxicity

Graphical Abstract

Authors

Jimit Shah, Florian Rouaud, Diego Guerrera, ..., Jan E. Carette, Manuel R. Amieva, Sandra Citi

Correspondence

sandra.citi@unige.ch

In Brief

Shah et al. clarify the mechanism through which adherens junctions render cells more susceptible to death by *S. aureus* α-toxin. PLEKHA7 and associated proteins create an Achilles heel by clustering the toxin receptor ADAM10 and toxin pores at junctions. Unclustered toxin pores are unstable and endocytosed, promoting cell survival.

Highlights

- The α-toxin receptor ADAM10 is clustered at junctions by the PLEKHA7-PDZD11 complex

- Tspan33 docks ADAM10 to junctions by binding to the WW domain of PLEKHA7

- ADAM10 junctional clustering promotes the efficient formation of stable toxin pores

- Loss of PLEKHA7-PDZD11 leads to toxin pore removal by endocytosis and cell survival

CellPress

A Dock-and-Lock Mechanism Clusters ADAM10 at Cell-Cell Junctions to Promote α-Toxin Cytotoxicity

Jimit Shah,[1,2] Florian Rouaud,[1,2] Diego Guerrera,[1,2] Ekaterina Vasileva,[1,2] Lauren M. Popov,[3] William L. Kelley,[4] Eric Rubinstein,[5] Jan E. Carette,[3] Manuel R. Amieva,[3] and Sandra Citi[1,2,6,*]

[1]Department of Cell Biology, Faculty of Sciences, University of Geneva, 1211-4 Geneva, Switzerland
[2]Institute for Genetics and Genomics of Geneva (iGE3), University of Geneva, 1211-4 Geneva, Switzerland
[3]Department of Microbiology and Immunology, Stanford University School of Medicine, Stanford, CA 94305, USA
[4]Department of Microbiology and Molecular Medicine, Faculty of Medicine, University of Geneva, 1211-4 Geneva, Switzerland
[5]INSERM, Université Paris-Sud, UMRS_935, 94807 Villejuif Cedex, France
[6]Lead Contact
*Correspondence: sandra.citi@unige.ch
 https://doi.org/10.1016/j.celrep.2018.10.088

SUMMARY

We previously identified PLEKHA7 and other junctional proteins as host factors mediating death by *S. aureus* α-toxin, but the mechanism through which junctions promote toxicity was unclear. Using cell biological and biochemical methods, we now show that ADAM10 is docked to junctions by its transmembrane partner Tspan33, whose cytoplasmic C terminus binds to the WW domain of PLEKHA7 in the presence of PDZD11. ADAM10 is locked at junctions through binding of its cytoplasmic C terminus to afadin. Junctionally clustered ADAM10 supports the efficient formation of stable toxin pores. Instead, disruption of the PLEKHA7-PDZD11 complex inhibits ADAM10 and toxin junctional clustering. This promotes toxin pore removal from the cell surface through an actin- and macropinocytosis-dependent process, resulting in cell recovery from initial injury and survival. These results uncover a dock-and-lock molecular mechanism to target ADAM10 to junctions and provide a paradigm for how junctions regulate transmembrane receptors through their clustering.

INTRODUCTION

Epithelial cells lining mucosal surfaces and skin constitute the primary barrier against bacterial and viral infections. Pathogens use different strategies to colonize and invade tissues, and bacteria can exert their cytotoxicity by secreting toxins. Pore-forming toxins, the largest class of bacterial toxins, are secreted in a soluble extracellular form and bind to transmembrane host receptors, leading to toxin oligomerization and insertion into the membrane as pores (Dal Peraro and van der Goot, 2016). Pore formation causes influx of calcium and loss of cellular ATP and potassium, leading to cell death by apoptosis and/or necrosis (Essmann et al., 2003). α-Toxin (Berube and Bubeck Wardenburg, 2013) is a potent virulence factor of *Staphylococcus aureus* and binds to the metalloprotease ADAM10 (a disintegrin and metalloproteinase domain-containing protein 10) (Wilke and Bubeck Wardenburg, 2010; Seilie and Bubeck Wardenburg, 2017). ADAM10, a single-pass transmembrane receptor, matures in a late Golgi compartment through the proteolytic cleavage of its pro-domain and is involved in many physiological and pathological processes (Seals and Courtneidge, 2003). The maturation of ADAM10, its exit from the endoplasmic reticulum, and its trafficking and surface expression are regulated by a group of tetraspanins referred to as tetraspanins-C8 (TspanC8s) (Matthews et al., 2017; Saint-Pol et al., 2017; Seipold and Saftig, 2016). Although it is hypothesized that TspanC8s target ADAM10 to different cell compartments, nothing is known about either the localization of TspanC8s at junctions or the mechanisms underlying their localizations.

Epithelial junctions are involved in host-pathogen interactions at multiple levels. Adherens junctions (AJs) maintain the integrity of epithelial sheets and provide an innate immunity barrier to pathogens. AJs comprise transmembrane adhesion proteins, cadherins and nectins, connected to the actin cytoskeleton by catenin and afadin protein complexes and to microtubules through PLEKHA7 (pleckstrin homology domain-containing, family A member 7) (Meng and Takeichi, 2009). In polarized epithelial cells, AJs comprise two spatially distinct domains: the *zonula adherens* (ZA), a circumferential apical belt immediately basal to tight junctions (TJs) that contains afadin and PLEKHA7 and an underlying actomyosin ring (Meng et al., 2008; Pulimeno et al., 2010; Kurita et al., 2013), and "lateral contacts," distributed basally to the ZA, that contain cadherins and catenins but lack afadin and PLEKHA7 (Pulimeno et al., 2010). TJs maintain a semi-permeable seal between cells that forms a barrier to the free diffusion of pathogens and toxins though the paracellular space (Guttman and Finlay, 2009). TJs comprise transmembrane proteins of the claudin and occludin and MARVEL (MAL and related proteins for vesicle trafficking and membrane link) families and immunoglobulin (Ig)-like adhesion molecules (Anderson and Van Itallie, 2009), which are connected

to the cytoskeleton through cytoplasmic plaque proteins (Guillemot et al., 2008). Importantly, transmembrane junctional proteins function as receptors for pathogens and toxins. For example, nectins, junctional adhesion molecule (JAM), claudins, and occludin can act either as receptors and/or barriers for viruses and toxins (Bergelson, 2009; Harris et al., 2010; Eichner et al., 2017; Guttman and Finlay, 2009). However, the role of cytoplasmic junctional proteins in host-pathogen interactions is poorly understood.

Surprisingly, a recent genetic screen in Hap1 cells identified PLEKHA7 and other AJ proteins as cellular host factors required for *Staphylococcus aureus* α-toxin-mediated cell death (Popov et al., 2015). When cells are treated with sub-lytic concentrations of α-toxin, PLEKHA7 knockout (KO) cells show a similar extent of initial injury as wild-type (WT) cells but eventually recover from the initial damage and survive, whereas ADAM10-KO cells survive with no injury (Popov et al., 2015). Thus, toxin pores can form in PLEKHA7-KO cells, consistent with normal levels of surface ADAM10 in these cells (Popov et al., 2015). PLEKHA7 is a zonula adhaerens (ZA) protein that forms a complex with other cytoplasmic junctional proteins, including afadin and PDZD11 (Meng et al., 2008; Pulimeno et al., 2010, 2011; Kurita et al., 2013; Guerrera et al., 2016; Shah et al., 2016). In Hap1 cells treated with α-toxin, the phenotype of PLEKHA7-KO cells was rescued by the N-terminal tryptophan-tryptophan (WW) and pleckstrin homology (PH) domains of PLEKHA7 (Popov et al., 2015), which are required for its interaction with PDZD11 (Guerrera et al., 2016) and afadin (Kurita et al., 2013), respectively, suggesting that these proteins act in a complex to regulate α-toxin toxicity. However, the molecular mechanism through which PLEKHA7 and other hits identified in the screen promote cell death upon α-toxin treatment remained unclear. Furthermore, although the ADAM10 partner Tspan33, a member of the TspanC8 family, was also identified as one of the top hits in the screen (Popov et al., 2015), there is no known interaction of Tspan33 with PLEKHA7 or any other junctional protein. Here we report that a new macromolecular complex, comprising Tspan33, PLEKHA7, PDZD11, and afadin, orchestrates the clustering of ADAM10 at junctions and promotes cell death through the efficient formation of stable, clustered α-toxin pores.

RESULTS

The Junctional Clustering of ADAM10 Correlates with Its Maturation, Cell Confluency, and α-Toxin-Dependent Cell Death

Using an antibody validated on cells depleted of ADAM10 (Figures S1A–S1D), we examined ADAM10 immunofluorescence (IF) localization in confluent kidney (mouse cortical collecting duct, mCCD) cells, grown on Transwell filters to enhance apico-basal polarization. ADAM10 was co-localized with PLEKHA7 at apical junctions (arrows, Figures 1A and 1B), which comprise the zonular junctions TJ and ZA, and where the respective markers ZO-1 and PLEKHA7 show partially overlapped localizations (Pulimeno et al., 2010; Vasileva et al., 2017). It should be noted that ZA proteins and some TJ proteins, including ZO-1 (Howarth et al., 1992), are localized

at AJs in non-epithelial cells, such as myeloblastic-derived Hap1 cells. In z-sections, ADAM10 was localized both at apical junctions (arrows, Figure 1B) and along lateral contacts (yellow arrowheads, Figure 1B), which lack PLEKHA7 and ZO-1 (white arrowheads, Figure 1B). Immunohistochemistry revealed ADAM10 signal co-localizing with PLEKHA7 and ZO-1 at junctions of lung and kidney epithelial cells (arrows, Figure 1C) and cytoplasmic staining (yellow arrowheads, Figure 1C). In WT but not ADAM10-KO Hap1 cells, intense ADAM10 labeling along AJ segments of the peripheral membrane was co-localized with PLEKHA7 and ZO-1 (arrows, Figure S1C, WT), whereas less intense labeling was detected in non-junctional areas and the cytoplasm (yellow arrowheads, Figure S1C, WT). In SKCO (ATCC HTB-39TM), Madin Darby canine kidney II (MDCKII), A427, A549, and mouse embryonic endothelial cells (meECs), we observed both junctional and/or zonular labeling (arrows, Figure S1E) and cytoplasmic and/or lateral labeling (yellow arrowheads, Figure S1E) for ADAM10, indicating that junctional clustering can occur in many types of junction-forming cells. Immunoblot (IB) analysis showed that ADAM10 migrates as two main polypeptides of molecular size (M_r) ~90 kDa and ~68 kDa, corresponding to immature and mature forms, respectively, in lysates of mCCD (Figure 1F; Figure S1B), Hap1 (Figure S1D), and other cell types (Figure S1F).

We asked whether the junctional distribution of ADAM10 correlates with ADAM10 maturation, cell confluency, and susceptibility to α-toxin (Figures 1D–1H). Although PLEKHA7 was already exclusively detected at junctions after 2 days of culture (arrows, Figure 1D), the localization of ADAM10 progressively shifted from cytoplasmic fibrillar structures (yellow arrowheads, Figure 1D) to cell-cell junctions as confluency increased between 2 and 6 days of culture (arrows, Figure 1D; quantification in Figure 1E, top). Conversely, cytoplasmic ADAM10 labeling decreased with increasing confluence (yellow arrowheads, Figure 1D; quantification in Figure 1E, bottom). IB analysis showed that the accumulation of ADAM10 at junctions correlated with an increased proportion of the mature form versus the immature form (Figure 1F; quantification in Figure 1G). Treatment of cultures with α-toxin showed that increased junctional accumulation of ADAM10 correlated with increased cell death following α-toxin treatment (Figure 1H). In summary, these results indicate that epithelial cell confluency correlates with increases in the accumulation and clustering of ADAM10 at junctions, the levels of the mature ~68 kDa form of ADAM10, and cellular susceptibility to α-toxin. Taken together, these observations suggest that clustering of mature ADAM10 at junctions promotes α-toxin cytotoxic activity.

PLEKHA7 Is Required for ADAM10 Junctional Clustering

To test whether PLEKHA7 controls ADAM10 junctional clustering, we generated PLEKHA7-KO mCCD cells (Figures S2A–S2C) and examined ADAM10 localization in mixed cultures of WT and KO cells, to directly compare neighboring cells (Figures 2A and 2B). In WT cells, ADAM10 was localized both sharply at zonular junctions, co-localizing with PLEKHA7 (white arrows, Figures 2A and 2B), and along lateral membranes (yellow arrowheads, Figures 2A and 2B). In PLEKHA7-KO cells, no ADAM10 labeling was colocalized with zonular proteins (white arrowheads
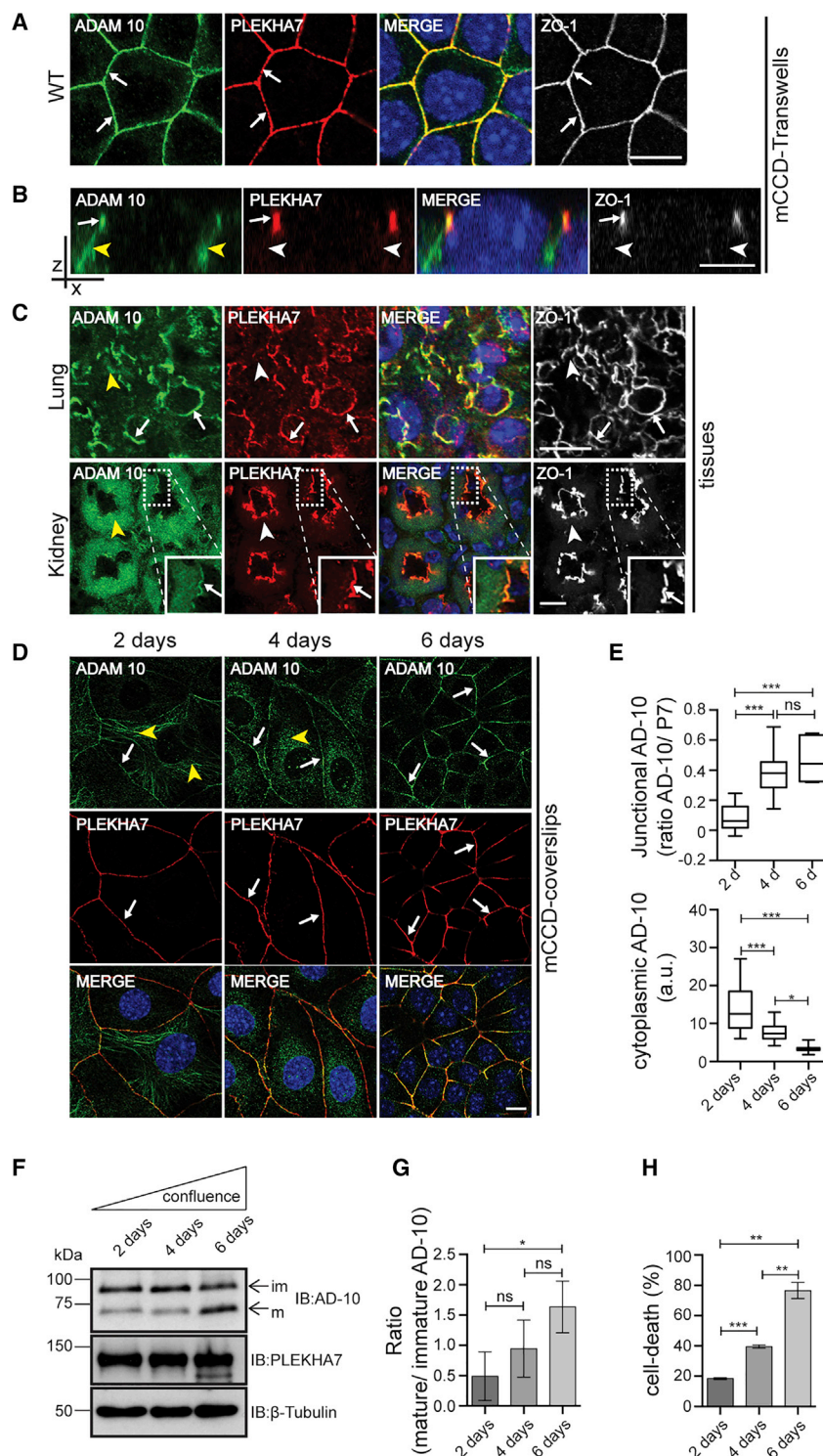
Figure 1. Junctional Clustering of ADAM10 Correlates with Cell Density, ADAM10 Maturation, and Cellular Susceptibility to *S. aureus* α-Toxin

(A–D) ADAM10 localization by immunofluorescence (IF) in mCCD cells (A, B, and D) and mouse frozen sections (C). PLEKHA7 and ZO-1 label zonular junctions (ZAs and TJs). The substrate for cell culture is indicated on the right. Merge images show nuclei labeled in blue (DAPI). Cells were imaged on the XY plane (A) or XZ plane (B). White arrows indicate co-localization at zonular junctions, white arrowheads indicate reduced or undetectable junctional staining, and yellow arrowheads indicate either lateral (B) or cytoplasmic (D) localization. Scale bars 20 μm.

(E) Semiquantitative analysis of junctional labeling intensity for ADAM10, ratioed to PLEKHA7 (E, top) or cytoplasmic ADAM10 (a.u., E, bottom). Asterisks indicate statistical significance.

(F and G) IB analysis (F) and densitometric quantification (G) of mature (m, ∼68 kDa) versus immature (im, ∼90 kDa) ADAM10. PLEKHA7 and β-tubulin were used to normalize protein loading. The numbers on the left indicate migration of molecular weight (MW) markers (kilodaltons).

(H) Percentages of cell death (PI staining) upon intoxication of WT mCCD cells as a function of confluency.

Data are represented as either median (E) or mean (G and H) ± SEM. *p < 0.05, **p < 0.01, ***p < 0.001. See also Figure S1.

demonstrating that the phenotype is not due to clonal variation and off-target effects. The loss of PLEKHA7 did not cause dramatic changes in junctional architecture in either cell type, based on the localization of E-cadherin (arrows, Figures S2B and S2D), ZO-1 (arrows, Figure 2A; Figures S2E and S2G), and other markers (data not shown), indicating that the altered localization of ADAM10 is not the result of a major disruption of junctional architecture. In PLEKHA7-KO Hap1 cells, ADAM10 clustering at cell contacts (AJ) was undetectable (white arrowheads, Figure S2G). Neither KO nor depletion of PLEKHA7 affected either total levels or maturation of ADAM10 in mCCD (Figure 2C; Figure S2F) and Hap1 cells (Figure S2H), in agreement with the normal levels of ADAM10 detected on the surface of PLEKHA7-KO Hap1 cells (Popov et al., 2015). Together, these observations suggest that ADAM10 maturation does not require its clustering at junctions,

and magnified inset, Figure 2B), whereas the lateral membrane distribution was not affected (yellow arrowheads, Figures 2A and 2B). Loss of zonular ADAM10 was observed in different KO clonal lines (Figure S2D) and in small interfering RNA (siRNA)-PLEKHA7-depleted cells (Figures S2E and S2F), and that junctional ADAM10 redistributes to the lateral pool upon KO of PLEKHA7.

Next we rescued the localization of ADAM10 in PLEKHA7-KO mCCD cells by re-expressing exogenous yellow fluorescent protein (YFP)-tagged PLEKHA7 full-length (FL) and mutant
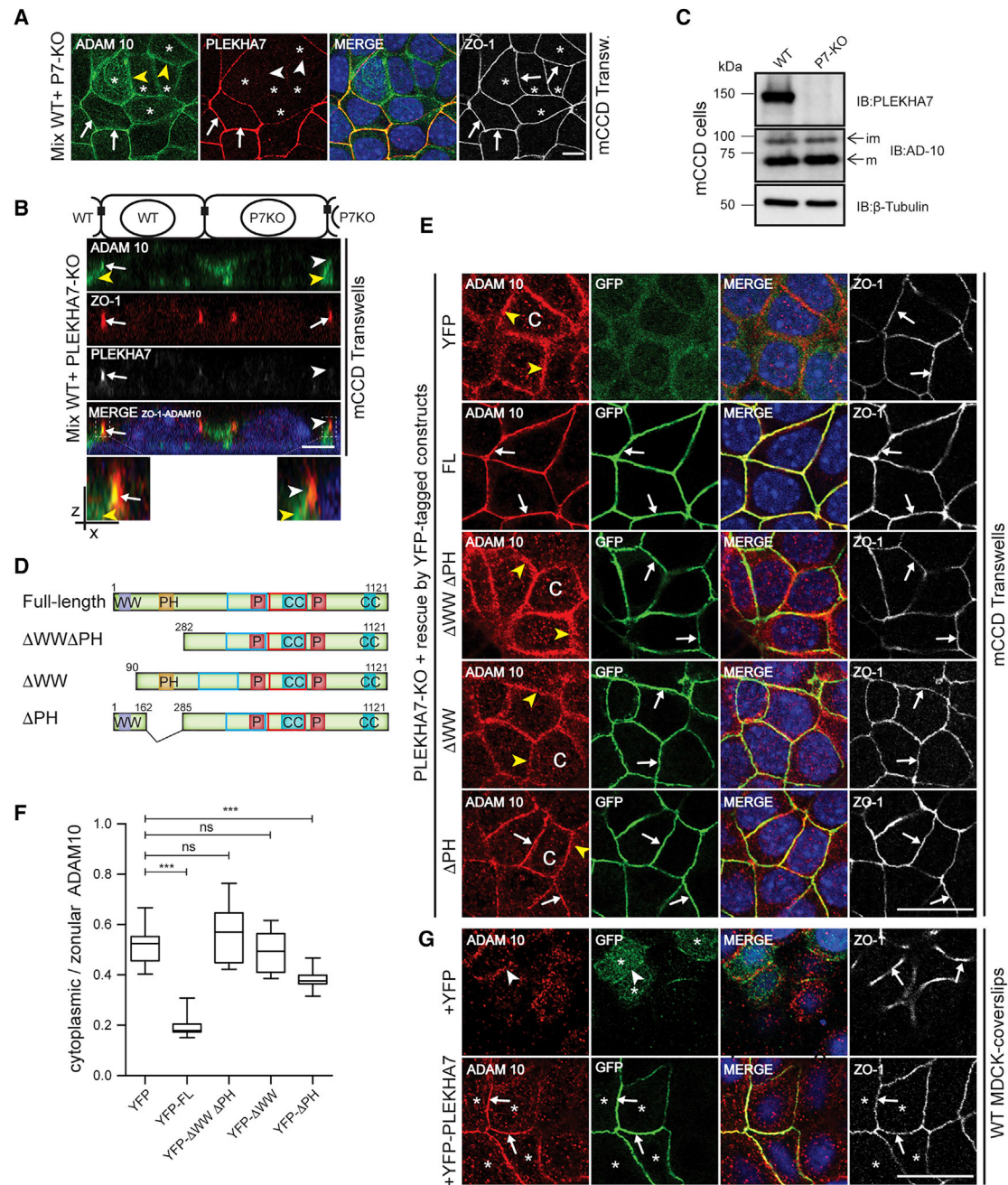
Figure 2. PLEKHA7 WW Domains Are Required for Junctional Clustering of ADAM10

(A and B) IF localization of ADAM10 either in mixed cultures of WT and PLEKHA7-KO mCCD cells in either the XY plane (A) or XZ plane (B).

(C) IB analysis of im and m ADAM10 in WT or PLEKHA7-KO cell lysates.

(D–F) IF localization of ADAM10 in PLEKHA7-KO cells transfected with YFP-tagged constructs (scheme in D and IF images in E; "C"=cytoplasmic ADAM10 in E) and (F) semiquantitative analysis of cytoplasmic versus junctional ADAM10 in PLEKHA7-KO cells as a function of the rescue construct.

(G) ADAM10 localization in WT MDCK cells transfected with either YFP alone or YFP-PLEKHA7.

Asterisks indicate cells knocked out for PLEKHA7 (A) or statistical significance (median ± SEM) (F) or cells positive for transfection (G). Scale bars, 20 μm (A, E, and G) or 5 μm (B). ***p < 0.001. See also Figure S2.

constructs, all of which were targeted to zonular junctions (arrows, Figure 2E; Paschoud et al., 2014). FL PLEKHA7 completely restored the clustered zonular localization of ADAM10 in PLEKHA7-KO cells (arrows, Figure 2E, FL; quantification in Figure 2F). The WW and PH domains of PLEKHA7 are required for its interaction with PDZD11 (Guerrera et al., 2016) and afadin (Kurita et al., 2013), respectively. A PLEKHA7 deletion mutant lacking both the WW and PH domains (ΔWWΔPH) did not rescue
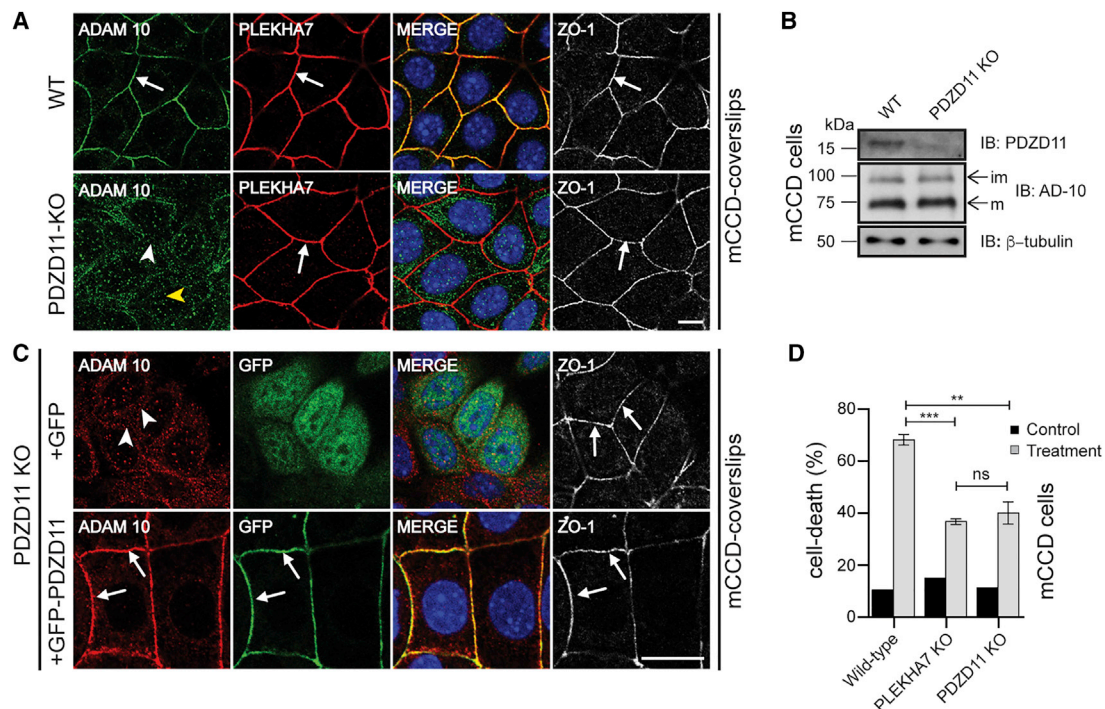
Figure 3. PDZD11 Is Required for PLEKHA7-Dependent Junctional ADAM10 Docking
(A and C) IF localization of ADAM10 either in mCCD WT (A, top) or PDZD11-KO (A, bottom) cells or cells rescued with either GFP alone or GFP-PDZD11 (C).
(B) IB analysis of im and m ADAM10 in either WT or PDZD11-KO cell lysates.
(D) Percentage of cell death upon α-toxin treatment (mean ± SEM).
**p < 0.01, ***p < 0.001. See also Figure S3.

ADAM10 localization, which was indistinguishable from cells rescued with GFP alone, with a predominant diffuse localization along lateral junctions, and cytoplasmic labeling (yellow arrowheads and "C" Figure 2E, ΔWWΔPH; quantification in Figure 2F). Cells rescued with the mutant lacking the tandem WW domains showed no zonular labeling of ADAM10 but showed lateral and cytoplasmic labeling (yellow arrowheads, Figure 2E, ΔWW; quantification in Figure 2F). Cells expressing the mutant lacking the PH domain showed partial recovery of zonular labeling for ADAM10 and some cytoplasmic labeling (arrows, Figure 2E, ΔPH; quantification in Figure 2F). Overexpression of FL PLEKHA7 in MDCK cells, which express low levels of endogenous PLEKHA7 compared with mCCD cells (Vasileva et al., 2017), increased the intensity of ADAM10 zonular labeling (arrows, Figure 2G).

Together, these results indicate that PLEKHA7 does not regulate the expression, maturation, trafficking, and surface delivery of ADAM10, but it controls ADAM10 docking to junctions, through a mechanism that depends primarily on its WW domains, and partially on the PH domain, both of which are required to rescue toxicity (Popov et al., 2015). In contrast, the WW domains alone are not targeted to junctions (Figure S2I) and does not rescue toxicity (Popov et al., 2015). This indicates that junctional clustering of ADAM10 by the PLEKHA7 WW domains requires targeting of the WW domains to junctions, through the binding of downstream sequences to junctional proteins, and is critically important for α-toxin cytotoxicity.

PLEKHA7 Clusters ADAM10 through PDZD11

The WW domains of PLEKHA7 are required to recruit PDZD11 to junctions (Guerrera et al., 2016), and PDZD11 was identified in the Hap1 screen (Popov et al., 2015). To validate the implication of PDZD11, we examined ADAM10 localization in PDZD11-KO mCCD cells (Guerrera et al., 2016; Figure 3) and Hap1 cells (Figure S3). In PDZD11-KO mCCD cells, ADAM10 lost its zonular localization (white arrowhead, Figure 3A) and showed increased non-junctional staining (yellow arrowhead, Figure 3A), whereas PLEKHA7 and ZO-1 were not affected (arrows, Figure 3A). KO of PDZD11 did not modify the levels of mature versus immature forms of ADAM10 (Figure 3B). In Hap1 cells, KO of PDZD11 (Figures S3A and S3B) resulted in loss of the clustered localization of ADAM10 at junctions (arrowheads, Figure S3C). This phenotype was rescued by expression of exogenous GFP-tagged PDZD11 (arrows, Figure 3C). These observations show that ADAM10 clustering by PLEKHA7 requires PDZD11.

Next we examined the effect of KO of either PLEKHA7 or PDZD11 on α-toxin-mediated cell death, assessed by propidium iodide (PI) staining. Hap1 cells KO for PLEKHA7 show decreased cell death at sub-lytic doses of α-toxin (Popov et al., 2015). Here we show that mCCD cells (Figure 3D) and Hap1 cells (Figure S3D) knocked out for either PLEKHA7 or PDZD11 also show decreased cell death at sub-lytic doses of α-toxin. Pore-dependent cellular injury was assessed by measuring intracellular ATP levels after treatment with increasing doses of α-toxin (10, 20, 30, and 40 U/mL). In ADAM10-KO cells there was no loss of

intracellular ATP up to 24 hr of toxin treatment, regardless of the dose (Figures S3E–S3H), consistent with no pore formation. In cells knocked out for either PLEKHA7 or PDZD11, at the lowest toxin dose (10 U/mL) the fall in intracellular ATP was almost undetectable (Figure S3E). At intermediate toxin doses (20 and 30 U/mL), ATP levels initially fell in PLEKHA7-KO and PDZD11-KO Hap1 cells, similar to WT cells, but at approximately 4 hr after treatment, ATP levels started to recover (Figures S3F and S3G). The kinetics of ATP loss in the first 3 hr of treatment indicated a slightly faster drop in ATP levels in WT cells compared with cells KO for either PLEKHA7 or PDZD11, suggesting more efficient pore formation in WT cells. At high toxin doses (40 U/mL), neither PLEKHA7-KO nor PDZD11-KO cells showed a significant recovery of ATP levels up to 24 hr post-intoxication, similar to WT cells (Figure S3H).

Together, these results demonstrate that PLEKHA7 acts through PDZD11 to cluster ADAM10 at junctions, and that cells knocked out for either PLEKHA7 or PDZD11 are resistant to low, but not to high toxin doses, suggesting that pores of WT cells are more cytotoxic.

Tetraspanin33 Docks ADAM10 to Junctions through Its LEL and C-Terminal Cytoplasmic Tail

The trafficking, maturation, and surface expression of ADAM10 depends on the C8 sub-family of tetraspanins (TspanC8). TspanC8s contain cytoplasmic N and C termini, four transmembrane domains, and a short and a large extracellular loop (LEL), this latter interacting with the extracellular domain of ADAM10 (Dornier et al., 2012; Jouannet et al., 2016; Saint-Pol et al., 2017; Prox et al., 2012; Noy et al., 2016; Haining et al., 2012). Tspan33, a member of TspanC8s, was identified as a key host factor required for α-toxin cytotoxicity (Popov et al., 2015). To explore the involvement of TspanC8s in ADAM10 localization, we first examined TspanC8 expression in mCCD cells by microarray analysis. All TspanC8s were expressed in mCCD cells, and TSPAN15 gene expression increased 3.8-fold upon KO of PLEKHA7 (Figure S4A). Next, because antibodies to label endogenous tetraspanins are not available, we analyzed the localization of exogenously expressed GFP-tagged Tspans (Dornier et al., 2012). Tspan15 and Tspan33 accumulated at the cell periphery in mCCD cells (arrows, Figure S4B), whereas Tspan5, Tspan10, Tspan14, and Tspan17 were predominantly cytoplasmic (yellow arrowheads, Figure S4B). In polarized mCCD cells, Tspan15 was not detected in the apical plane, marked by PLEKHA7 and apical E-cadherin (white arrowheads and arrows, Figures 4A and 4B), but was distributed along lateral contacts, marked by ADAM10 and lateral E-cadherin, but not PLEKHA7 (yellow arrowheads, Figures 4A and 4B; scheme in Figure 4E). In contrast, GFP-Tspan33 was detected at apical junctions, co-localizing with PLEKHA7 (white arrows, Figures 4C and 4D), but not along lateral membranes (white arrowheads, Figures 4C and 4D; scheme in Figure 4E). The junctional accumulation of Tspan33 was increased in confluent cells (Figures S4C and S4D), similar to ADAM10 (Figures 1D and 1E). To examine the role of Tspan33 in more detail, we characterized Tspan33-KO Hap1 cells (Popov et al., 2015; Figure S4E) and showed that KO of Tspan33 did not affect the protein levels

and the maturation of ADAM10 (Figures S4F and S4G), suggesting that Tspan33 is not essential for the synthesis and proteolytic maturation of ADAM10. However, ADAM10 lost its clustered junctional labeling upon KO of Tspan33 in Hap1 cells (white arrowheads, Figure S4H), demonstrating that Tspan33 is required for the junctional docking of ADAM10. In agreement, overexpression of Tspan33 increased the accumulation of ADAM10 at junctions of WT cells (double arrows, Figures S4I–S4K).

To identify the regions of Tspan33 that are involved in clustering ADAM10 at junctions, we generated chimeric molecules where either the LEL or the cytoplasmic C-terminal tail of either Tspan15, Tspan33, or CD82 (Tspan27) was exchanged with that of another Tspan (schemes, Figures 4F and S4L). CD82 was chosen as a negative control because its LEL contains 6 cysteine residues, similar to Tspan33, but it does not interact with ADAM10 (Dornier et al., 2012). These constructs were expressed in the background of Tspan33-KO Hap1 cells (Figure 4F) and WT mCCD cells (Figure S4L). WT Tspan15 and CD82 were distributed along all of the surface of Hap1 cells (double arrows, Figure 4F), whereas Tspan33 was clustered at PLEKHA7-containing junctions (arrow, Figure 4F). Tspan15 and Tspan33, but not CD82, recruited ADAM10 to either the whole cell surface or to PLEKHA7-containing contacts, respectively (double and single arrows, Figure 4F). The C-terminal region of Tspan33 was sufficient to drive Tspan15 to zonular junctions in mCCD cells (Figure S4L) and to cluster ADAM10 at PLEKHA7-containing junctions in Hap1 cells (arrow, Figure 4F, Tspan15:Tspan33C-term). Replacing the LEL of Tspan33 with the LEL of CD82 resulted in junctional localization of the chimera, but ADAM10 recruitment was strongly reduced (arrowhead, Figure 4F, Tspan33:CD82-LEL). Conversely, replacing the LEL of CD82 with the LEL of Tspan33 resulted in localization of the chimera all over the cell surface, similar to CD82 alone, without associated ADAM10 (double arrows, Figure 4F, CD82: Tspan33-LEL). Finally, inserting both the LEL and C-terminal region of Tspan33 into the backbone of CD82 resulted in recruitment of both the chimera and ADAM10 at junctions (arrows, Figure 4F, CD82: Tspan33-LEL-Cterm). Together, these observations indicate that the C-terminal region of Tspan33 is sufficient for the junctional docking of chimeras, the LEL of Tspan33 is necessary but not sufficient for ADAM10 interaction and junctional docking, and ADAM10 junctional docking requires the LEL of a TspanC8 combined with the C-terminal region of Tspan33.

The PLEKHA7-PDZD11 Complex Clusters ADAM10 at Junctions through Tspan33

Next, we reasoned that because Tspan33 is a key regulator of ADAM10 localization, the PLEKHA7-PDZD11 complex may control ADAM10 localization through Tspan33. We therefore examined the role of PLEKHA7 and PDZD11 in Tspan33 localization. In cells knocked out for either PLEKHA7 or PDZD11, the zonular localization of exogenous Tspan33 in mCCD cells was either undetectable or significantly reduced, and most of the labeling was detected diffusely in the cytoplasm and over the cell surface (arrowheads, Figure 5A; quantification in Figure 5B). In z-sections, Tspan33 was accumulated at zonular

Figure 4. The Large Extracellular Loop and the Cytoplasmic C-Terminal Regions of Tspan33 Are Necessary and Sufficient for ADAM10 Recruitment to Junctions

(A–E) IF and localization scheme (E) of exogenous GFP-tagged Tspan15 (T15) (A, XY plane; B, XZ plane) and GFP-Tspan33 (T33) (C, XY plane; D, XZ plane) in polarized WT mCCD cells.

(F) Structure-function analysis of Tspan33 through chimeric molecules expressed in Tspan33-KO Hap1 cells. Schemes of GFP-tagged Tspan WT and chimeric constructs are shown on the left (LEL, large extracellular loop; Cterm, cytoplasmic C-terminal region) and their IF localization and that of ADAM10 and PLEKHA7 (junctional marker) on the right.

Scale bar, 10 μm (A, C, and F) and 5 μm (B and D). See also Figure S4.

Figure 5. The PLEKHA7-PDZD11 Complex Recruits Tetraspanin 33 to Junctions

(A, C, and D) IF localization of GFP-Tspan33 in either WT or indicated KO mCCD cell lines imaged either on the XY (A) or XZ plane (C) or in Hap1 cells (D).

(B) Quantifications of junctional versus cytoplasmic and/or lateral GFP-Tspan33 related to (A) (mean ± SEM). **p < 0.01 and ***p < 0.001. See also Figure S4.

of ADAM10 occurs through PLEKHA7-PDZD11-dependent junctional docking of Tspan33.

Junctional Clustering of α-Toxin Pores by the PLEKHA7-PDZD11 Complex Promotes Cell Death through Stabilization by the Cytoskeleton and Protection from Macropinocytosis

Next, we investigated the mechanisms through which ADAM10 junctional clustering leads to increased cell death. First we examined the formation and dynamics of toxin pores, using an antib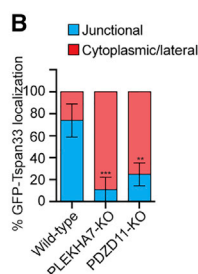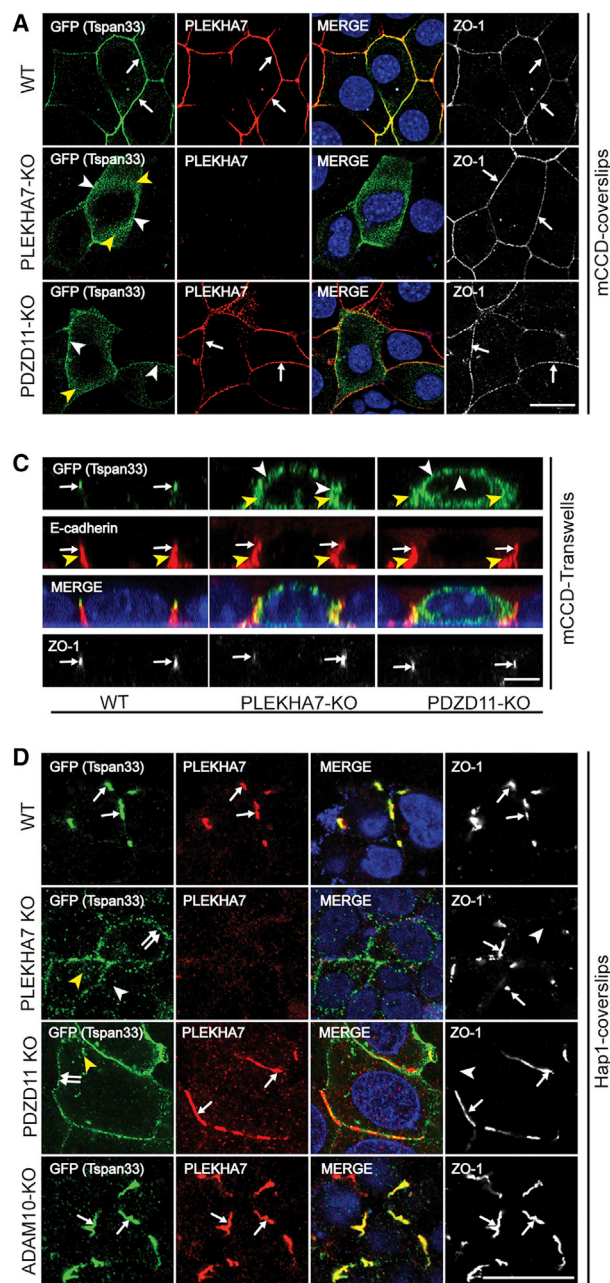ody against α-toxin validated by IF and IB analysis (Figures S5A and S5B), and live imaging with a fluorescently labeled toxin (Virreira Winter et al., 2016). α-Toxin-treated cells showed clustered toxin co-localized with PLEKHA7 (arrows, Figure S5A, middle panel), and no labeling was detected in ADAM10-KO Hap1 cells (arrowheads, Figure S5A, bottom panel), consistent with the lack of formation of pores in the absence of the receptor. In mCCD cells, toxin labeling was co-localized with ZO-1 in the apical plane (arrows, Figure 6A, WT, apical), and diffuse labeling was detected along lateral membranes lacking ZO-1 (yellow arrowheads, Figure 6A, WT, lateral), indicating that the localizations of toxin pores and ADAM10 overlap (see also Figure 1B). In cells knocked out for either PLEKHA7 or PDZD11, little or no clustered toxin was observed on the apical plane (white arrowheads, Figure 6A, apical, PLEKHA7-KO and PDZD11-KO; quantification in Figure 6B), whereas labeling was observed along lateral membranes, indistinguishable from WT cells (yellow arrowheads, Figure 6A, lateral). IB analysis showed that the total levels of α-toxin heptamers were similar in WT and KO mCCD cells (Figure 6C). This suggests that disruption of the PLEKHA7-PDZD11 complex affects pore assembly at junctions, but not along the lateral membrane. To examine the localization and stability of α-toxin, we carried out a time course and/or pulse-chase analysis of toxin localization in Hap1 cells (Figures

junctions in WT cells (arrows, Figure 5C), but in cells knocked out or depleted for either PLEKHA7 or PDZD11, no zonular labeling was detected, and Tspan33 was distributed throughout the plasma membrane and cytoplasm (arrowheads, Figure 5C; Figure S4M). KO of either PLEKHA7 or PDZD11 in Hap1 cells resulted in a diffuse localization of Tspan33 all over the cell surface (double arrows, Figure 5D) instead of a clustered co-localization with ZO-1 (arrows and arrowheads, Figure 5D). KO of ADAM10 did not affect the clustered accumulation of Tspan33 at junctions (arrows, Figure 5D), demonstrating that Tspan33 is docked to junctions independently of ADAM10. Collectively, these results indicate that junctional recruitment

Figure 6. PLEKHA7 and PDZD11 Are Required for the Formation of Stable α-Toxin Pores at Cell-Cell Junctions

(A and B) IF localization of α-toxin in either WT or KO mCCD cells (1 hr treatment) and imaged either at the apical (A, top) or lateral (A, bottom) plane and related semiquantitative analysis of junctional α-toxin labeling, ratioed to ZO-1 (B).

(C) IB (top) and densitometric quantifications (bottom) of α-toxin heptamers.

(D–F) IF localization of α-toxin in either WT (D), PLEKHA7-KO (E), or PDZD11-KO (F) Hap1 cells at different time points after α-toxin treatment and recovery after toxin removal.

(legend continued on next page)

6D–6F). Cells were treated with α-toxin for either 5 min or 30 min, and at the end of the 30-min treatment, α-toxin was removed, and cells were allowed to recover for 4 hr. α-Toxin was detectable at cell-cell contacts of WT Hap1 cells after 5 min (arrows, Figure 6D, 5 min; quantification in Figure S5C), suggesting rapid binding. The intensity of labeling increased after 30 min (arrows, Figure 6D, 30 min; quantification in Figure S5C), indicating increased accumulation of α-toxin pores. Importantly, in WT cells labeling remained clearly detectable at sites of cell-cell contact 4 hr after α-toxin removal from the medium (arrows, Figure 6D, WT, recovery; quantification in Figure S5C), indicating that when they are formed, junctional pores are stable. In contrast, labeling for α-toxin was detected at few junctional areas in PLEKHA7-KO Hap1 cells after 5 min of treatment, and labeling was less intense than in WT cells (arrows, Figure 6E, 5 min; quantification in Figure S5C), did not increase in intensity after 30 min of treatment (arrows, Figure 6E, 30 min; quantification in Figure S5C), and was undetectable after 4 hr of recovery (arrowheads, Figure 6E, recovery; quantification in Figure S5C). No toxin labeling was detected at junctions in PDZD11-KO Hap1 cells (arrowheads, Figure 6F; quantification in Figure S5C). In live Hap1 cells incubated with fluorescently labeled α-toxin (Virreira Winter et al., 2016), strong junctional labeling for α-toxin was detected after 30-min and 60-min treatment (arrows, Figure S5D, WT). In PLEKHA7-KO cells, weak labeling by fluorescent α-toxin was detectable at 30 min of treatment, and no labeling was detected at later times, as shown by the 60-min snapshot (yellow arrowheads, Figure S5D, PLEKHA7-KO), suggesting that pores do not efficiently assemble at junctions in the absence of PLEKHA7, and that the ones that do are unstable, in agreement with results from fixed cells. In contrast, in PDZD11-KO cells no clustered labeling was detected at cell contacts at any time point (yellow arrowheads, Figure S5D, PDZD11-KO). Importantly, in live cells α-toxin and GFP-Tspan33 were co-localized at sites of cell-cell contact (arrows, Figure S5E). Confirming results from fixed cells (Figure 5D), the localization of Tspan33 in live Hap1 cells was independent of ADAM10 (white arrow, Figure S5E, ADAM10-KO), but GFP-Tspan33 was detected over the whole cell surface and in the cytoplasm of overexpressing cells upon KO of either PLEKHA7 or PDZD11 (yellow arrowheads, Figure S5E). Correspondingly, labeling for α-toxin was discontinuous and only co-localized with Tspan33 at sites where Tspan33 labeling was strongest (yellow arrowheads, Figure S5E, PDZD11-KO). In Hap1 cells knocked out for Tspan33, no labeling for toxin was detected at junctions (arrowheads, Figure S5F), correlating with essentially no cell death, comparable to ADAM10-KO cells (Figure S5G). Together, these results indicate that clustering of Tspan33-ADAM10 at junctions by the PLEKHA7-PDZD11 complex leads to the formation of stable

toxin pores and enhanced cytotoxicity. In contrast, in the absence of either PLEKHA7 or PDZD11, the efficiency of junctional pore formation is drastically reduced, and the few junctional pores detected in PLEKHA7-KO cells are unstable.

To determine biochemically the decrease in the amount of α-toxin pores detectable on the cell surface of KO cells, rather than total pores, we performed a cell surface biotinylation assay. Following treatment of Hap1 cells with α-toxin, cells were cultured for 6 hr in the absence of α-toxin, then biotinylated for 30 min. and lysed. Analysis of total lysates showed that WT Hap1 cells and cells knocked out for either PLEKHA7 or PDZD11 showed similar levels of total α-toxin heptamers (Figure 6G, total), similar to what was observed for mCCD cells (Figure 6C). ADAM10-KO cells, used as a negative control, showed background levels of signal, because of non-specific labeling (Figure 6G). In contrast, surface levels of toxin were reduced by 50% in PLEKHA7-KO cells, when compared to WT cells, and almost to background (ADAM10-KO) levels in PDZD11-KO cells (Figure 6G). This suggests that α-toxin pores in cells lacking either PLEKHA7 or PDZD11 are more efficiently removed from the whole cell surface, whereas in WT cells, they persist on the cell surface.

To explore the mechanisms that regulate toxin pore stability, we used drugs to perturb the actin cytoskeleton and inhibit endocytosis. TJs and AJs contain a highly organized submembrane actomyosin cytoskeleton, that is tethered to afadin, α-catenin, and ZO-1 (Takeichi, 2014). Transmembrane junctional proteins are protected from endocytic internalization through mechanisms that implicate actin filaments (Shen and Turner, 2005; Le et al., 1999; Hoshino et al., 2005; Yap et al., 2007). Importantly, α-toxin pores are removed from the surface of HaCat cells by endocytosis, implicating endocytosis as a mechanism involved in membrane repair and cell survival after intoxication (Husmann et al., 2009). Treating cells with latrunculin-A (Lat-A), which disrupts actin filaments and prevents their polymerization, resulted in reduced clustering of toxin and shortening of junctional segments in Hap1 cells (arrows, Figure 6H). Correspondingly, Lat-A treatment resulted in reduced cell death (Figure 6I), indicating that the correct organization of cytoplasmic junctional proteins by actin filaments is required for the clustering of ADAM10, and the formation of highly cytotoxic pores. Next we used wortmannin and amiloride, two inhibitors of macropinocytosis (Koivusalo et al., 2010), to explore the role of endocytosis in cell death. Wortmannin treatment did not affect the percentage of cell death of toxin-treated WT cells, but increased the percentage of death of PLEKHA7-KO cells (Figure 6J). Amiloride treatment also resulted in a significant increase in cell death in PLEKHA7-KO cells, and a smaller increase in WT cells (Figure 6K). These results suggest that increased

(G) IB analysis of surface and total α-toxin heptamers either in WT or KO Hap1 cells, treated (top 2 panels) and non-treated (bottom 2 panels) with α-toxin. The red asterisks indicate non-specific background labeling, detected regardless of α-toxin treatment. The numbers below the blots show densitometric quantification of one representative experiment.
(H and I) IF localization of α-toxin and junctional markers in Hap1 cells treated with α-toxin either in the presence or absence of Lat-A (H) and percentage of cell death (I).
(J and K) Percentage of cell death upon α-toxin treatment of WT or KO Hap1 cells in the presence or absence of either wortmannin (J) or amiloride (K).
Data are represented as either median (B) or mean (C and I–K) ± SEM. **p < 0.01, ***p < 0.001. See also Figure S5.

Figure 7. PDZD11 Promotes Direct Binding of PLEKHA7 with Tspan33

(A–D) PLA assay of mCCD cells WT (top) or PDZD11-KO (bottom) with the indicated antibodies for either PLEKHA7-PDZD11 (A), PLEKHA7-ADAM10 (B), PLEKHA7-Tspan33 (C), or with ADAM10-Tspan33 (D). IF localization of GFP-Tspan33 (cells marked by asterisks) is shown on the right in (C) and (D). Arrows indicate a PLA signal (red dots) at junctions. White arrowheads indicate background or reduced labeling.

(E and F) IB analysis of immunoprecipitates (IPs) from lysates of either WT or PDZD11-KO Hap1 cells using either ADAM10 (E) or PLEKHA7 (F) for IP. Antibodies used for IP and IB are indicated on the top and right, respectively.

(legend continued on next page)

macropinocytosis is involved in the survival of PLEKHA7-KO cells treated with α-toxin.

Afadin Enhances ADAM10 Clustering by Maintaining Junctional Integrity

Afadin is essential for the organization of AJs (Ikeda et al., 1999; Mandai et al., 1997; Zhadanov et al., 1999), it interacts with PLEKHA7 (Kurita et al., 2013) and ZO-1 (Yamamoto et al., 1997), and was identified in the screen (Popov et al., 2015). To understand the involvement of afadin, we analyzed afadin-KO Hap1 cell clones (Popov et al., 2015; Figures S6A and S6B). Although in WT cells PLEKHA7, ZO-1, ADAM10, Tspan33 and α-toxin were co-localized along linear segments of cell-cell contacts (Figures S6A, S6C, S6E, and S6G, top, WT), in afadin-KO cells they were detected as discontinuous short segments and dots (Figures S6A, S6C, S6E, and S6G, bottom, KO; quantification in Figure S6D). Of notice, in afadin-KO cells some junctions that were labeled strongly for ZO-1 were not labeled for either PLEKHA7 or ADAM10 (red arrows and arrowheads, Figure S6C, afadin-KO, bottom). Conversely, other regions were positive for PLEKHA7 and α-toxin but negative for ZO-1 (white arrows and arrowheads, Figure S6E, afadin-KO and 6× magnified insets). These observations indicate that afadin holds together ZO-1- and PLEKHA7-containing complexes. Treatment of afadin-KO clones with α-toxin resulted in a decrease in cell death; however, the decrease was not as strong as that observed in PLEKHA7-KO cells (Figure S6F). Because fragmented clusters containing PLEKHA7, ADAM10, Tspan33 and toxin were detected in afadin-KO cells (arrows, Figures S6C and S6G, afadin-KO), this indicates that the ADAM10-Tspan33-PLEKHA7-PDZD11 complex still promotes the formation of cytotoxic pores in afadin-KO cells, although not as efficiently as in the context of junctions organized by afadin.

PDZD11 Promotes the Association of PLEKHA7 with the Tspan33-ADAM10 Complex, and Afadin Binds Directly to ADAM10

Because the junctional docking of ADAM10 and Tspan33 depends on PLEKHA7 and PDZD11, we asked whether they form a complex in vivo and interact in vitro. Using a proximity ligation (PLA) assay in WT mCCD cells, we observed a junctional signal between PLEKHA7 and PDZD11 (arrows, Figure 7A, top, positive control; Guerrera et al., 2016), PLEKHA7 and ADAM10 (arrows, Figure 7B, top), PLEKHA7 and Tspan33 (Figure 7C, top), and ADAM10 and Tspan33 (arrows, Figure 7D, top). These results indicate that these four proteins are physically proximal at junctions. In contrast, in cells knocked out for PDZD11, the PLA signal was significantly reduced, indicating that the proximity of PLEKHA7 with both Tspan33 and ADAM10 requires PDZD11 (arrowheads, Figures 7A–7D, bottom; quantification in Figures S7A–S7C). To characterize the molecular composition

of the PLEKHA7-based complex, we first analyzed ADAM10 immunoprecipitates (IPs). Afadin, PLEKHA7, and PDZD11 were detected in ADAM10 IPs from WT Hap1 cells, indicating that they form a complex (Figure 7E, WT). In contrast, afadin was detected but PLEKHA7 was not detected above background in ADAM10 IPs from PDZD11-KO cells (Figure 7E, PDZD11-KO). Next we immunoprecipitated PLEKHA7 from lysates of Hap1 cells expressing exogenous GFP-Tspan33. GFP-Tspan33 was detectable in PLEKHA7 IPs from WT cells but not from PDZD11-KO cells (Figure 7F; quantification in Figure S7D). Taken together, PLA and co-immunoprecipitation (coIP) experiments indicate that PLEKHA7 forms a complex with both ADAM10 and Tspan33, and that the formation of this complex requires PDZD11, in agreement with the IF results. Furthermore, ADAM10 can form a complex with afadin in vitro independently of PLEKHA7 and PDZD11.

Next we carried out GST pull-down assays using as bait either the cytoplasmic C-terminal region of ADAM10 or the cytoplasmic C-terminal region of TSPAN33 (Figures 7G, 7I, and 7J, baits in red). As preys, we used either constructs of the N-terminal region of PLEKHA7 (Figure 7G), or afadin (Figure 7I), or ZO-1 (Figure 7J). In addition, we tested the effect of PDZD11 on the interaction between the C-terminal regions of either ADAM10 or Tspan33 and the N-terminal constructs of PLEKHA7, by adding either CFP-hemagglutinin (HA) or PDZD11-HA (Figure 7G; normalization in Figure 7H, third molecule in blue) to the pull-down. Although full-length PDZD11, used as a positive control, interacted strongly with both the WW (1–162) and WW+PH (1–500) domains of PLEKHA7 (Guerrera et al., 2016), the baits consisting of either the cytoplasmic region of ADAM10 or the cytoplasmic C terminus of Tspan33 showed different behaviors (Figure 7G). The cytoplasmic region of ADAM10 did not bind to the WW (1–162) fragment above background, bound very weakly to the WW+PH (1–500) fragment, and this interaction was slightly enhanced in the presence of PDZD11 (dashed green box, Figure 7G). In contrast, the C-terminal region of Tspan33 showed binding to both the WW (1–162) and the N-terminal (N-term, 1–500) fragments of PLEKHA7, and both of these interactions were strongly enhanced in the presence of PDZD11 (solid green box, Figure 7G). Both PDZD11 and the cytoplasmic C-terminal region of Tspan33 interacted with the complete WW domain, which comprises tandem WW sequences (W1+W2), but they did not interact with the isolated W2 sequence of PLEKHA7, which does not bind to PDZD11 (Guerrera et al., 2016; Figure S7E), suggesting that the W1 region of PLEKHA7 is required for its PDZD11-mediated interaction with the C-terminal region of Tspan33. The N terminus of Tspan33 did not interact with the WW (1–162) fragment of PLEKHA7 (Figure S7F).

To determine whether the C-terminal cytoplasmic regions of either ADAM10 or Tspan33 bind to either afadin or ZO-1, we carried out additional pull-downs, using PLEKHA7 and nectin

(G–J) IB analysis of GST pull-downs carried out using bacterially expressed GST fusion baits (red) and preys (green, the antibody for IB is indicated on the right) expressed either in HEK293 cells (G) or insect cells (I and J). Ponceau S-stained blots show bait normalization. The third protein for tri-molecular pull-downs is shown in blue (normalization shown in H). Prey, dashed and continuous green boxes; baits, dashed black boxes.

(K) Scheme of macromolecular junctional complex comprising Tspan33, ADAM10, α-toxin pores, PLEKHA7, PDZD11, and afadin. Nectin and E-cadherin are included as molecular components of AJs.

See also Figure S7.

as positive control baits for afadin, and occludin for ZO-1, respectively. The C terminus of ADAM10 interacted with full-length afadin (green box, Figure 7I) but not ZO-1 (Figure 7J), whereas the C terminus of Tspan33 did not interact with either (Figures 7I and 7J). Moreover, the C termini of ADAM10 and Tspan33 did not interact with PDZD11 alone (Figures S7G and S7H). Finally, we mapped the ADAM10-binding region of afadin to its N-terminal, Ras-association (RA)-domain-containing region (Figures S7I and S7J), and identified PLEKHA7, ADAM10, and PDZD11 in afadin IPs (Figure S7K). In summary, these results indicate that the N-terminus of PLEKHA7 interacts *in vitro* with the C terminus of Tspan33 in a PDZD11-dependent manner, and that the N terminus of afadin interacts directly with the C terminus of ADAM10 (Figure 7K), indicating that afadin can lock ADAM10 at junctions, when ADAM10 has been docked there via the PDZD11-dependent interaction of Tspan33 with PLEKHA7.

DISCUSSION

Understanding the host-dependent molecular mechanisms that control toxin virulence is essential to develop rational approaches for the prevention and treatment of bacterial infections. Here we show that a new macromolecular complex (Figure 7K) clusters the α-toxin receptor ADAM10 to junctions by a dock-and-lock mechanism involving Tspan33, PLEKHA7, PDZD11 and afadin, thus promoting efficient cell death by *S. aureus* α-toxin. Clustering of transmembrane proteins is essential to support the major canonical functions of epithelial apical junctions, such as adhesion, which is driven by adhesion receptor clustering (Wu et al., 2015), and TJ barrier function, which requires claudin clustering and polymerization (Umeda et al., 2006). Furthermore, junctional complexes cross-talk with different types of receptors, that can cluster at junctions, and thus control downstream signaling pathways (Lampugnani et al., 2006; Pellon-Cardenas et al., 2013). Here we show that the function of ADAM10, a transmembrane receptor implicated in a variety of physiological and pathological processes (Seals and Courtneidge, 2003; Dornier et al., 2012; Saint-Pol et al., 2017) and a nucleator of α-toxin pores, is also regulated by clustering at cell-cell junctions.

Previous studies reported a junctional localization of ADAM10 in MDCK cells (Wild-Bode et al., 2006) and keratinocytes (Husmann et al., 2009). We extend these observations by describing different pools of ADAM10: a zonular and/or junctional pool, localized at the ZA in polarized epithelial (mCCD) cells and AJ of Hap1 cells, which requires the PLEKHA7-PDZD11 complex; a lateral or non-junctional surface membrane pool, which is not clustered by PLEKHA7-PDZD11; and a cytoplasmic pool. The relative distribution of ADAM10 into these pools depends on cell and tissue type, probably depending on TspanC8 member expression and/or localization, and the degree of confluency. Thus, in cultured epithelial cells, high confluency promotes the zonular accumulation of ADAM10, its maturation, and cell death following toxin treatment. This agrees with the observation that epithelial cells are sensitive to α-toxin only when they are confluent and establish cell-cell contacts (Kwak et al., 2012). ADAM10 is delivered to the cell surface via interaction of its

extracellular domains with the LEL of TspanC8s (Dornier et al., 2012; Noy et al., 2016). By using chimeric molecules, we show that the cytoplasmic C-terminal tail of Tspan33 is crucial for its junctional localization, but that both the C terminus and the LEL are required for efficient recruitment of ADAM10 to junctions. Our experiments collectively demonstrate that Tspan33 mediates docking of ADAM10 to junctions, through the PDZD11-dependent interaction of its cytoplasmic domain with PLEKHA7. These results provide a new role for the PLEKHA7-PDZD11 complex, and identify Tspan33 as a new transmembrane junctional protein. Finally, we identify a role for afadin, which is to lock ADAM10 at junctions, by binding directly to the ADAM10 cytoplasmic domain. The locking requires previous docking of Tspan33 by PLEKHA7-PDZD11, because it does not occur in cells knocked out for either PLEKHA7 or PDZD11. The stabilizing effect of afadin is highlighted by the observation that the localization of ADAM10 in PLEKHA7-KO cells is not fully rescued by PLEKHA7 constructs that lack the PH domain, which is involved in PLEKHA7 interaction with afadin (Kurita et al., 2013). Because afadin linkage to actin filaments is essential for its function (Sakakibara et al., 2018), we conclude that afadin helps to anchor the PLEKHA7-PDZD11-ADAM10 complex to the actin cytoskeleton, stabilizing both junctions and toxin pores.

Our study provides new mechanistic insights into the biology of tetraspanins, which organize membrane microdomains and are involved in many physiological and pathological processes (Hemler, 2008). Although ADAM10 co-localizes with discrete TspanC8s at the plasma membrane of lymphoid, HeLa, and osteosarcoma cells (U2OS) (Arduise et al., 2008; Dornier et al., 2012; Jouannet et al., 2016) and in endosomes (Schröder et al., 2009; Seipold et al., 2017), it is not known how TspanC8s are localized, and whether they target ADAM10 to different plasma membrane domains, including cell-cell junctions. Here we show that the cytoplasmic C terminus of Tspan33 docks it to junctions, through the PDZD11-mediated binding to the WW domains of PLEKHA7, providing the first evidence of a molecular mechanism of tetraspanin subcellular targeting. Both Tspan conformation and assembly into Tspan-enriched microdomains (TEMs) (Charrin et al., 2003; Silvie et al., 2006) and α-toxin oligomerization into pores (Tomita et al., 1992) critically require cholesterol. Significantly, proteins that control cholesterol biosynthesis and metabolism were identified as hits in our screen for host factors that control α-toxin cytotoxicity (Popov et al., 2015). Our interpretation is that cholesterol is required for enhanced α-toxin cytotoxicity because of its role in controlling the function of Tspans and, hence, the PLEKHA7-PDZD11-dependent docking of ADAM10 to junctions.

We show that junctional clustering of ADAM10 results in enhanced pore toxicity, and we provide evidence for two topologically and functionally distinct types of pores: zonular and/or junctional pores, which depend on junctional ADAM10 and on the integrity of the Tspan33-PLEKHA7-PDZD11-afadin complex, and lateral or non-junctional pores, which promote early injury and cell death independent of PLEKHA7-PDZD11 and afadin, when the toxin dose is high. Because similar amounts of heptamers are formed when comparing WT cells with cells knocked out for either PLEKHA7 or PDZD11 (see also Popov

et al., 2015), we conclude that PLEKHA7, PDZD11 and afadin act primarily by regulating the junctional clustering of ADAM10, and not by affecting total pore levels or downstream signaling pathways leading to cell death, because these latter would likely be affected regardless of the topological origin of the initial cellular injury. Indeed, the kinetics of loss of ATP, which provides a direct readout of pore activity, are not dramatically different during early phases of intoxication from high toxin doses, when comparing WT with PLEKHA7-KO or PDZD11-KO cells. This suggests that pores nucleated by non-junctional and junctional pools of ADAM10 cause cell death through similar mechanisms (see also Popov et al., 2015). However, because cell death occurs in cells lacking PLEKHA7 when the toxin dose is sufficiently high (see also Popov et al., 2015), we conclude that non-junctional pores induce an intrinsically weaker injury than junctional pores. Thus, at sub-lytic doses of toxin, repair mechanisms are sufficient to limit cell damage before an irreversible threshold is reached, and cells survive. In contrast, at high toxin doses, the saturation of the non-junctional pool of ADAM10 is sufficient to induce cell death, overcoming repair mechanisms. Little is known about the cell repair mechanisms leading to survival after treatment with α-toxin. Data from HaCat cells showed that endocytosis plays a role in toxin removal from the cell surface (Hussmann et al., 2009). Consistent with the notion that the junctional actin cytoskeleton protects junctional transmembrane proteins from endocytosis (Shen and Turner, 2005; Le et al., 1999; Hoshino et al., 2005; Yap et al., 2007), we observed that treatment with Lat-A reduced α-toxin clustering, and increased the survival of WT Hap1 cells. Our observation that inhibitors of macropinocytosis promote death of PLEKHA7-KO cells treated with α-toxin indicates that the increased survival of KO cells is at least in part due to increased macropinocytosis. The concept that pore stability at junctions mediates efficient cytotoxicity is supported by our IF observations, showing that clustered junctional pores in WT cells persist for hours at the cell surface after removal of toxin, indicating that they provide a sustained injury. Instead, in PLEKHA7-KO cells, although total pores are similar to WT cells, the surface levels of toxin, as determined both by IF and biotinylation assays, rapidly decrease, correlating with cell survival after the initial injury. Another possible mechanism through which clustering of ADAM10 promotes toxicity is by enhancing the initial formation of toxin heptamers. This mechanism is supported by the differences observed between WT and either PLEKHA7-KO or PDZD11-KO cells, with respect to kinetics of ATP loss and the decreased junctional accumulation of toxin at early time points in KO cells, as determined by IF. Collectively, our results support a model whereby clustering of ADAM10 at junctions renders cells more vulnerable to the cytotoxic activity of α-toxin by promoting efficient formation of pores, and by hindering the endocytic cellular repair mechanisms that lead to pore removal.

In summary, we describe a new macromolecular complex of cytoplasmic junctional proteins, that orchestrates the function of the transmembrane receptor ADAM10, by docking and locking it at junctions. These results provide new mechanistic insights into the diverse signaling functions of cytoplasmic junctional proteins, the regulation of the cellular distribution and signaling outputs of ADAM10 and tetraspanins, and the importance of subcellular localization and spatial arrangement in the activity of pore-forming toxins.

STAR★METHODS

Detailed methods are provided in the online version of this paper and include the following:

- KEY RESOURCES TABLE
- CONTACT FOR REAGENT AND RESOURCE SHARING
- EXPERIMENTAL MODEL AND SUBJECT DETAILS
- METHOD DETAILS
  - Genome Engineering
  - Microarray analysis
  - Antibodies and Plasmids
  - Immunofluorescence, Immunohistochemistry and Proximity Ligation Assay
  - Cell transfections and siRNA-mediated depletion
  - Sample preparation, SDS-PAGE and Immunoblot analysis
  - Cell surface biotinylation
  - Co-Immunoprecipitation assay
  - GST pulldowns
  - Intoxication, cell viability assay and flow cytometry
  - Pharmacological inhibition of cellular processes
  - Confocal microscopy and live-cell imaging
- QUANTIFICATION AND STATISTICAL ANALYSIS
  - Analysis of immunofluorescence (IF) signals:
  - Analysis of immunoblotting data
  - PLA signal quantifications
  - Cell-death analysis

REFERENCES

Anderson, J.M., and Van Itallie, C.M. (2009). Physiology and function of the tight junction. Cold Spring Harb. Perspect. Biol. *1* (*2, a002584*), a002584.

Arduise, C., Abache, T., Li, L., Billard, M., Chabanon, A., Ludwig, A., Mauduit, P., Boucheix, C., Rubinstein, E., and Le Naour, F. (2008). Tetraspanins regulate ADAM10-mediated cleavage of TNF-alpha and epidermal growth factor. J. Immunol. *181*, 7002–7013.

Bergelson, J.M. (2009). Intercellular junctional proteins as receptors and barriers to virus infection and spread. Cell Host Microbe *5*, 517–521.

Berube, B.J., and Bubeck Wardenburg, J. (2013). Staphylococcus aureus α-toxin: nearly a century of intrigue. Toxins (Basel) *5*, 1140–1166.

Bolstad, B.M., Irizarry, R.A., Astrand, M., and Speed, T.P. (2003). A comparison of normalization methods for high density oligonucleotide array data based on variance and bias. Bioinformatics *19*, 185–193.

Cassidy, P., and Harshman, S. (1979). Characterization of detergent-solubilized iodine-125-labeled alpha-toxin bound to rabbit erythrocytes and mouse diaphragm muscle. Biochemistry *18*, 232–236.

Charrin, S., Manié, S., Thiele, C., Billard, M., Gerlier, D., Boucheix, C., and Rubinstein, E. (2003). A physical and functional link between cholesterol and tetraspanins. Eur. J. Immunol. *33*, 2479–2489.

Cordenonsi, M., Mazzon, E., De Rigo, L., Baraldo, S., Meggio, F., and Citi, S. (1997). Occludin dephosphorylation in early development of Xenopus laevis. J. Cell Sci. *110*, 3131–3139.

Cordenonsi, M., D'Atri, F., Hammar, E., Parry, D.A., Kendrick-Jones, J., Shore, D., and Citi, S. (1999). Cingulin contains globular and coiled-coil domains and interacts with ZO-1, ZO-2, ZO-3, and myosin. J. Cell Biol. *147*, 1569–1582.

Dal Peraro, M., and van der Goot, F.G. (2016). Pore-forming toxins: ancient, but never really out of fashion. Nat. Rev. Microbiol. *14*, 77–92.

Dornier, E., Coumailleau, F., Ottavi, J.F., Moretti, J., Boucheix, C., Mauduit, P., Schweisguth, F., and Rubinstein, E. (2012). TspanC8 tetraspanins regulate ADAM10/Kuzbanian trafficking and promote Notch activation in flies and mammals. J. Cell Biol. *199*, 481–496.

Eichner, M., Protze, J., Piontek, A., Krause, G., and Piontek, J. (2017). Targeting and alteration of tight junctions by bacteria and their virulence factors such as Clostridium perfringens enterotoxin. Pflugers Arch. *469*, 77–90.

Essmann, F., Bantel, H., Totzke, G., Engels, I.H., Sinha, B., Schulze-Osthoff, K., and Jänicke, R.U. (2003). Staphylococcus aureus alpha-toxin-induced cell death: predominant necrosis despite apoptotic caspase activation. Cell Death Differ. *10*, 1260–1272.

Guerrera, D., Shah, J., Vasileva, E., Sluysmans, S., Méan, I., Jond, L., Poser, I., Mann, M., Hyman, A.A., and Citi, S. (2016). PLEKHA7 Recruits PDZD11 to Adherens Junctions to Stabilize Nectins. J. Biol. Chem. *291*, 11016–11029.

Guillemot, L., Paschoud, S., Pulimeno, P., Foglia, A., and Citi, S. (2008). The cytoplasmic plaque of tight junctions: a scaffolding and signalling center. Biochim. Biophys. Acta *1778*, 601–613.

Guttman, J.A., and Finlay, B.B. (2009). Tight junctions as targets of infectious agents. Biochim. Biophys. Acta *1788*, 832–841.

Haining, E.J., Yang, J., Bailey, R.L., Khan, K., Collier, R., Tsai, S., Watson, S.P., Frampton, J., Garcia, P., and Tomlinson, M.G. (2012). The TspanC8 subgroup of tetraspanins interacts with A disintegrin and metalloprotease 10 (ADAM10) and regulates its maturation and cell surface expression. J. Biol. Chem. *287*, 39753–39765.

Harris, H.J., Davis, C., Mullins, J.G., Hu, K., Goodall, M., Farquhar, M.J., Mee, C.J., McCaffrey, K., Young, S., Drummer, H., et al. (2010). Claudin association with CD81 defines hepatitis C virus entry. J. Biol. Chem. *285*, 21092–21102.

Hemler, M.E. (2008). Targeting of tetraspanin proteins–potential benefits and strategies. Nat. Rev. Drug Discov. *7*, 747–758.

Hochberg, Y., and Benjamini, Y. (1990). More powerful procedures for multiple significance testing. Stat. Med. *9*, 811–818.

Hoshino, T., Sakisaka, T., Baba, T., Yamada, T., Kimura, T., and Takai, Y. (2005). Regulation of E-cadherin endocytosis by nectin through afadin, Rap1, and p120ctn. J. Biol. Chem. *280*, 24095–24103.

Howarth, A.G., Hughes, M.R., and Stevenson, B.R. (1992). Detection of the tight junction-associated protein ZO-1 in astrocytes and other nonepithelial cell types. Am. J. Physiol. *262*, C461–C469.

Husmann, M., Beckmann, E., Boller, K., Kloft, N., Tenzer, S., Bobkiewicz, W., Neukirch, C., Bayley, H., and Bhakdi, S. (2009). Elimination of a bacterial pore-forming toxin by sequential endocytosis and exocytosis. FEBS Lett. *583*, 337–344.

Ikeda, W., Nakanishi, H., Miyoshi, J., Mandai, K., Ishizaki, H., Tanaka, M., Togawa, A., Takahashi, K., Nishioka, H., Yoshida, H., et al. (1999). Afadin: A key molecule essential for structural organization of cell-cell junctions of polarized epithelia during embryogenesis. J. Cell Biol. *146*, 1117–1132.

Jouannet, S., Saint-Pol, J., Fernandez, L., Nguyen, V., Charrin, S., Boucheix, C., Brou, C., Milhiet, P.E., and Rubinstein, E. (2016). TspanC8 tetraspanins differentially regulate the cleavage of ADAM10 substrates, Notch activation and ADAM10 membrane compartmentalization. Cell. Mol. Life Sci. *73*, 1895–1915.

Koivusalo, M., Welch, C., Hayashi, H., Scott, C.C., Kim, M., Alexander, T., Touret, N., Hahn, K.M., and Grinstein, S. (2010). Amiloride inhibits macropinocytosis by lowering submembranous pH and preventing Rac1 and Cdc42 signaling. J. Cell Biol. *188*, 547–563.

Kurita, S., Yamada, T., Rikitsu, E., Ikeda, W., and Takai, Y. (2013). Binding between the junctional proteins afadin and PLEKHA7 and implication in the formation of adherens junction in epithelial cells. J. Biol. Chem. *288*, 29356–29368.

Kwak, Y.K., Vikström, E., Magnusson, K.E., Vécsey-Semjén, B., Colque-Navarro, P., and Möllby, R. (2012). The Staphylococcus aureus alpha-toxin perturbs the barrier function in Caco-2 epithelial cell monolayers by altering junctional integrity. Infect. Immun. *80*, 1670–1680.

Lampugnani, M.G., Orsenigo, F., Gagliani, M.C., Tacchetti, C., and Dejana, E. (2006). Vascular endothelial cadherin controls VEGFR-2 internalization and signaling from intracellular compartments. J. Cell Biol. *174*, 593–604.

Le, T.L., Yap, A.S., and Stow, J.L. (1999). Recycling of E-cadherin: a potential mechanism for regulating cadherin dynamics. J. Cell Biol. *146*, 219–232.

Mandai, K., Nakanishi, H., Satoh, A., Obaishi, H., Wada, M., Nishioka, H., Itoh, M., Mizoguchi, A., Aoki, T., Fujimoto, T., et al. (1997). Afadin: A novel actin filament-binding protein with one PDZ domain localized at cadherin-based cell-to-cell adherens junction. J. Cell Biol. *139*, 517–528.

Matthews, A.L., Szyroka, J., Collier, R., Noy, P.J., and Tomlinson, M.G. (2017). Scissor sisters: regulation of ADAM10 by the TspanC8 tetraspanins. Biochem. Soc. Trans. *45*, 719–730.

Meng, W., and Takeichi, M. (2009). Adherens junction: molecular architecture and regulation. Cold Spring Harb. Perspect. Biol. *1*, a002899.

Meng, W., Mushika, Y., Ichii, T., and Takeichi, M. (2008). Anchorage of microtubule minus ends to adherens junctions regulates epithelial cell-cell contacts. Cell *135*, 948–959.

Noy, P.J., Yang, J., Reyat, J.S., Matthews, A.L., Charlton, A.E., Furmston, J., Rogers, D.A., Rainger, G.E., and Tomlinson, M.G. (2016). TspanC8 Tetraspanins and A Disintegrin and Metalloprotease 10 (ADAM10) Interact via Their Extracellular Regions: EVIDENCE FOR DISTINCT BINDING MECHANISMS FOR DIFFERENT TspanC8 PROTEINS. J. Biol. Chem. *291*, 3145–3157.

Paschoud, S., Jond, L., Guerrera, D., and Citi, S. (2014). PLEKHA7 modulates epithelial tight junction barrier function. Tissue Barriers *2*, e28755.

Pellon-Cardenas, O., Clancy, J., Uwimpuhwe, H., and D'Souza-Schorey, C. (2013). ARF6-regulated endocytosis of growth factor receptors links cadherin-based adhesion to canonical Wnt signaling in epithelia. Mol. Cell. Biol. *33*, 2963–2975.

Popov, L.M., Marceau, C.D., Starkl, P.M., Lumb, J.H., Shah, J., Guerrera, D., Cooper, R.L., Merakou, C., Bouley, D.M., Meng, W., et al. (2015). The adherens junctions control susceptibility to Staphylococcus aureus α-toxin. Proc. Natl. Acad. Sci. USA *112*, 14337–14342.

Prox, J., Willenbrock, M., Weber, S., Lehmann, T., Schmidt-Arras, D., Schwanbeck, R., Saftig, P., and Schwake, M. (2012). Tetraspanin15 regulates cellular trafficking and activity of the ectodomain sheddase ADAM10. Cell. Mol. Life Sci. *69*, 2919–2932.

Pulimeno, P., Bauer, C., Stutz, J., and Citi, S. (2010). PLEKHA7 is an adherens junction protein with a tissue distribution and subcellular localization distinct from ZO-1 and E-cadherin. PLoS ONE *5*, e12207.

Pulimeno, P., Paschoud, S., and Citi, S. (2011). A role for ZO-1 and PLEKHA7 in recruiting paracingulin to tight and adherens junctions of epithelial cells. J. Biol. Chem. *286*, 16743–16750.

Ran, F.A., Hsu, P.D., Wright, J., Agarwala, V., Scott, D.A., and Zhang, F. (2013). Genome engineering using the CRISPR-Cas9 system. Nat. Protoc. *8*, 2281–2308.

Saint-Pol, J., Eschenbrenner, E., Dornier, E., Boucheix, C., Charrin, S., and Rubinstein, E. (2017). Regulation of the trafficking and the function of the metalloprotease ADAM10 by tetraspanins. Biochem. Soc. Trans. *45*, 937–944.

Sakakibara, S., Maruo, T., Miyata, M., Mizutani, K., and Takai, Y. (2018). Requirement of the F-actin-binding activity of l-afadin for enhancing the formation of adherens and tight junctions. Genes Cells *23*, 185–199.

Schröder, J., Lüllmann-Rauch, R., Himmerkus, N., Pleines, I., Nieswandt, B., Orinska, Z., Koch-Nolte, F., Schröder, B., Bleich, M., and Saftig, P. (2009). Deficiency of the tetraspanin CD63 associated with kidney pathology but normal lysosomal function. Mol. Cell. Biol. *29*, 1083–1094.

Seals, D.F., and Courtneidge, S.A. (2003). The ADAMs family of metalloproteases: multidomain proteins with multiple functions. Genes Dev. *17*, 7–30.

Seilie, E.S., and Bubeck Wardenburg, J. (2017). Staphylococcus aureus poreforming toxins: The interface of pathogen and host complexity. Semin. Cell Dev. Biol. *72*, 101–116.

Seipold, L., and Saftig, P. (2016). The Emerging Role of Tetraspanins in the Proteolytic Processing of the Amyloid Precursor Protein. Front. Mol. Neurosci. *9*, 149.

Seipold, L., Damme, M., Prox, J., Rabe, B., Kasparek, P., Sedlacek, R., Altmeppen, H., Willem, M., Boland, B., Glatzel, M., and Saftig, P. (2017). Tetraspanin 3: A central endocytic membrane component regulating the expression of ADAM10, presenilin and the amyloid precursor protein. Biochim Biophys Acta Mol Cell Res *1864*, 217–230.

Shah, J., Guerrera, D., Vasileva, E., Sluysmans, S., Bertels, E., and Citi, S. (2016). PLEKHA7: Cytoskeletal adaptor protein at center stage in junctional organization and signaling. Int. J. Biochem. Cell Biol. *75*, 112–116.

Shen, L., and Turner, J.R. (2005). Actin depolymerization disrupts tight junctions via caveolae-mediated endocytosis. Mol. Biol. Cell *16*, 3919–3936.

Silvie, O., Charrin, S., Billard, M., Franetich, J.F., Clark, K.L., van Gemert, G.J., Sauerwein, R.W., Dautry, F., Boucheix, C., Mazier, D., and Rubinstein, E. (2006). Cholesterol contributes to the organization of tetraspanin-enriched microdomains and to CD81-dependent infection by malaria sporozoites. J. Cell Sci. *119*, 1992–2002.

Spadaro, D., Le, S., Laroche, T., Mean, I., Jond, L., Yan, J., and Citi, S. (2017). Tension-dependent stretching activates ZO-1 to control the junctional localization of its interactors. Curr. Biol. *27*, 3783–3795.

Takeichi, M. (2014). Dynamic contacts: rearranging adherens junctions to drive epithelial remodelling. Nat. Rev. Mol. Cell Biol. *15*, 397–410.

Tomita, T., Watanabe, M., and Yasuda, T. (1992). Influence of membrane fluidity on the assembly of Staphylococcus aureus alpha-toxin, a channelforming protein, in liposome membrane. J. Biol. Chem. *267*, 13391–13397.

Umeda, K., Ikenouchi, J., Katahira-Tayama, S., Furuse, K., Sasaki, H., Nakayama, M., Matsui, T., Tsukita, S., Furuse, M., and Tsukita, S. (2006). ZO-1 and ZO-2 independently determine where claudins are polymerized in tight-junction strand formation. Cell *126*, 741–754.

Vasileva, E., Sluysmans, S., Bochaton-Piallat, M.L., and Citi, S. (2017). Cellspecific diversity in the expression and organization of cytoplasmic plaque proteins of apical junctions. Ann. N Y Acad. Sci. *1405*, 160–176.

Virreira Winter, S., Zychlinsky, A., and Bardoel, B.W. (2016). Genome-wide CRISPR screen reveals novel host factors required for Staphylococcus aureus α-hemolysin-mediated toxicity. Sci. Rep. *6*, 24242.

Wild-Bode, C., Fellerer, K., Kugler, J., Haass, C., and Capell, A. (2006). A basolateral sorting signal directs ADAM10 to adherens junctions and is required for its function in cell migration. J. Biol. Chem. *281*, 23824–23829.

Wilke, G.A., and Bubeck Wardenburg, J. (2010). Role of a disintegrin and metalloprotease 10 in Staphylococcus aureus alpha-hemolysin-mediated cellular injury. Proc. Natl. Acad. Sci. USA *107*, 13473–13478.

Wu, Y., Kanchanawong, P., and Zaidel-Bar, R. (2015). Actin-delimited adhesion-independent clustering of E-cadherin forms the nanoscale building blocks of adherens junctions. Dev. Cell *32*, 139–154.

Yamamoto, T., Harada, N., Kano, K., Taya, S., Canaani, E., Matsuura, Y., Mizoguchi, A., Ide, C., and Kaibuchi, K. (1997). The Ras target AF-6 interacts with ZO-1 and serves as a peripheral component of tight junctions in epithelial cells. J. Cell Biol. *139*, 785–795.

Yap, A.S., Crampton, M.S., and Hardin, J. (2007). Making and breaking contacts: the cellular biology of cadherin regulation. Curr. Opin. Cell Biol. *19*, 508–514.

Zhadanov, A.B., Provance, D.W., Jr., Speer, C.A., Coffin, J.D., Goss, D., Blixt, J.A., Reichert, C.M., and Mercer, J.A. (1999). Absence of the tight junctional protein AF-6 disrupts epithelial cell-cell junctions and cell polarity during mouse development. Curr. Biol. *9*, 880–888.

STAR★METHODS

KEY RESOURCES TABLE

REAGENT or RESOURCE	SOURCE	IDENTIFIER
Antibodies		
Rabbit polyclonal anti-PLEKHA7	Citi Laboratory	R30388
Guinea pig polyclonal anti-PLEKHA7	Citi Laboratory	GP2737
Mouse monoclonal anti-PLEKHA7	Citi Laboratory	37-8-F1
Rabbit polyclonal anti-ADAM10	Merck Millipore	Cat# AB19026 RRID: AB_2242320
Mouse monoclonal anti-p120catenin	Reynolds Laboratory	15D2
Mouse monoclonal anti-E-cadherin	BD Biosciences	Cat# BD610181
Rat monoclonal anti-ZO1	ATCC	R40.76, RRID: AB_2205518
Rabbit polyclonal anti-afadin	Sigma-Aldrich	Cat# A0224 RRID: AB_257871
Mouse monoclonal anti-β-tubulin	Thermo Fisher Scientific	Cat# 71-1500, RRID: AB_2533977
Mouse monoclonal anti-GFP	Roche	Cat# 11814460001 RRID: AB_390913
Rabbit polyclonal anti-GFP	Thermo Fisher Scientific	Cat# A-11122 RRID: AB_221569
Rabbit polyclonal anti-PDZD11	Citi Laboratory	R29958
Mouse monoclonal anti-HA	Thermo Fisher Scientific	Cat# 32-6700, RRID: AB_2533092
Mouse monoclonal anti-myc	Gerard Evan, MRC LMB	Cat# 9E10, RRID: AB_2266850
Mouse monoclonal anti-FLAG	Sigma-Aldrich	Cat# F1804, RRID: AB_262044
Rabbit polyclonal anti-HIS	Santa Cruz	Cat# sc-803, RRID: AB_631655
Rabbit polyclonal anti- *S.aureus* α-toxin	Sigma-Aldrich	Cat# S7531 RRID: AB_261550
Alexa Fluor 488-AffiniPure Donkey Anti-Rabbit IgG	Jackson Laboratory	Cat# 711-545-152 RRID: AB_2313584
FITC -AffiniPure Goat Anti-Mouse IgG	Jackson Laboratory	Cat# 115-095-062 RRID: AB_2338594
Cy3-AffiniPure Donkey Anti-Rabbit IgG	Jackson Laboratory	Cat# 711-165-152 RRID: AB_2307443
Cy3-AffiniPure Donkey Anti-Mouse IgG	Jackson Laboratory	Cat# 715-165-151 RRID: AB_2315777
Alexa Fluor 647-AffiniPure Donkey Anti-Guinea Pig IgG	Jackson Laboratory	Cat# 706-605-148 RRID: AB_2340476
Cy5-AffiniPure Donkey Anti-Rat IgG	Jackson Laboratory	Cat# 712-175-153 RRID: AB_2340672
Anti-Mouse IgG (H+L), HRP conjugate	Promega	Cat# W4021 RRID: AB_430834
Anti-Rabbit IgG (H+L), HRP conjugate	Promega	Cat# W4011 RRID: AB_430833
Biological Samples		
α-Hemolysin from *Staphylococcus aureus* (α-toxin)	Sigma-Aldrich	Cat# H9395
Alexa647 tagged α-toxin	Zychlinsky Laboratory (Virreira Winter et al., 2016)	N/A
Chemicals, Peptides, and Recombinant Proteins		
Latrunculin A	Sigma-Aldrich	Cat# L5163
5-(N-Ethyl-N-isopropyl) amiloride	Sigma-Aldrich	Cat# A3085
Wortmannin	Cell Signaling Technology	Cat# 9951
Poly-L-Lysine solution	Sigma-Aldrich	Cat# P4707
GST-human ADAM10-Cterm	This paper	S1845
GST-human Tspan33-Nterm	This paper	S2262
GST-human Tspan33-Cterm	This paper	S2263
GST-human PLEKHA7-Nterm	This paper	S1192
GST- human Nectin-1-Cterm	This paper	S1890
GST-human PLEKHA7-WW	Citi Laboratory (Guerrera et al., 2016)	S1792
GST-human PDZD11	Citi Laboratory (Guerrera et al., 2016)	S1743
GST-*Xenopus* Occludin-C-term	Citi Laboratory (Cordenonsi et al., 1997)	S983

(*Continued on next page*)

Continued

REAGENT or RESOURCE	SOURCE	IDENTIFIER
Critical Commercial Assays		
Proximity Ligation Assay (PLA)	Sigma-Aldrich	Cat# DU092101
Pierce ™ Cell Surface Protein Isolation Kit	Thermo Fisher Scientific	Cat# 89881
CellTiter-Glo Luminescent cell viability assay kit	Promega	Cat# G7570
Lipofectamine 2000	Invitrogen	Cat# 11668027
Lipofectamine RNAiMAX	Invitrogen	Cat# 13778030
NucleoSpin RNA II kit	Macherey-Nagel	Cat# 740955.50
Experimental Models: Cell Lines		
Mouse cortical collecting duct cell line, mCCD-WT N64-Tet-ON	Feraille Laboratory, Unige	N/A
Mouse cortical collecting duct cell line, mCCD-PLEKHA7-KO N64-Tet-off	This paper	N/A
Mouse cortical collecting duct cell line, mCCD-PDZD11-KO N64-Tet-off	Citi Laboratory (Guerrera et al., 2016)	N/A
Human colon carcinoma cell line, SKCO-15-WT	Nusrat Laboratory, Emory Univ.	N/A
Human haploid cell lines, Hap1 (WT, PLEKHA7-KO, afadin-KO, Tspan33-KO and ADAM10-KO)	Amieva Laboratory (Popov et al., 2015)	N/A
Human haploid cell line, Hap1 (PDZD11-KO)	This paper	N/A
Mouse ciliated embryonic aorta-derived endothelial cell line, meECs	Kwak Laboratory, Unige	N/A
Canine kidney proximal tubule cell line, MDCK-II Tet-OFF	Fanning Laboratory, U. North Carolina	N/A
Human lung carcinoma cell lines (A427 and A549)	Paggi Laboratory, Regina Elena NCI, Rome	N/A
Human embryonic kidney HEK293T	ATCC	N/A
SF9 insect cell lines	Louise Fairall, MRC LMB	N/A
Experimental Models: Organisms/Strains		
BL21-DE3 Competent cells	NEB	Cat# C2530H
DH5-α Competent cells	Thermo Fisher	Cat# 18265017
DH10B Competent cells	Thermo Fisher	Cat# 18297010
Oligonucleotides		
si-RNA target sequence: mouse ADAM10 ATAAAGTACTTGATTATGA	This paper	N/A
si-RNA target sequence: mouse PLEKHA7 CTGATGACACCTACCTCCA	This paper	N/A
CRISPR target sequence: mouse PLEKHA7GCGACTACAAGTACGCACAG	This paper	N/A
CRISPR target sequence: human PDZD11 ATCACACTGAAGAAGCCTCC	This paper	N/A
Recombinant DNA		
pTRE2hyg-YFP PLEKHA7-myc	Citi Laboratory (Paschoud et al., 2014)	S1431
pTRE2hyg -YFP ΔWW ΔPH PLEKHA7-myc	Citi Laboratory (Paschoud et al., 2014)	S1433
pTRE2hyg -YFP ΔWW PLEKHA7-myc	This paper	S1825
pTRE2hyg -YFP ΔPH PLEKHA7-myc	This paper	S1826
pTRE2hyg -YFP WW PLEKHA7-myc	This paper	S1822
pTRE2hyg -YFP-myc	Citi Laboratory (Paschoud et al., 2014)	S1210
pcDNA3.1(+) GFP-human PDZD11-myc	Citi Laboratory (Guerrera et al., 2016)	S1761
pTRE2hyg human WW (WI+W2) PLEKHA7-myc	This paper	S2261
pTRE2hyg human N-term PLEKHA7	This paper	S1831
pTRE2hyg human W2 PLEKHA7-myc	This paper	S2260
pEGFP-N1 human Tspan5	Rubinstein Laboratory (Dornier et al., 2012)	S2149

(*Continued on next page*)

Continued

REAGENT or RESOURCE	SOURCE	IDENTIFIER
pEGFP-N1 human Tspan10	Rubinstein Laboratory (Dornier et al., 2012)	S2150
pEGFP-N3 human Tspan14	Rubinstein Laboratory (Dornier et al., 2012)	S2151
pEGFP-N3 human Tspan15	Rubinstein Laboratory (Dornier et al., 2012)	S2152
pEGFP-N1 human Tspan17	Rubinstein Laboratory (Dornier et al., 2012)	S2153
pEGFP-N1 human Tspan33	Rubinstein Laboratory (Dornier et al., 2012)	S2154
pEGFP-N3 mouse Tspan15	This paper	S2298
pEGFP-N3 mouse Tspan33	This paper	S2299
pEGFP-N3 mouse Tspan15:Tspan33 Cterm (chimera)	This paper	S2300
pEGFP-N1 human CD82	This paper	S2371
pEGFP-N1 human Tspan33:CD82-LEL (chimera)	This paper	S2372
pEGFP-N1 human CD82:Tspan33 -LEL (chimera)	This paper	S2373
pEGFP-N1 human CD82:Tspan33 -LEL-Cterm (chimera)	This paper	S2374
pFLAG-CMV rat afadin	Takai Laboratory (Kurita et al., 2013)	S2286
pFLAG-CMV rat afadin_NN	Takai Laboratory (Kurita et al., 2013)	S2289
pFLAG-CMV rat afadin_RA	Takai Laboratory (Kurita et al., 2013)	S2291
pFLAG-CMV rat afadin_NC	Takai Laboratory (Kurita et al., 2013)	S2290
pFLAG-CMV rat afadin_DIL	Takai Laboratory (Kurita et al., 2013)	S2293
pFastBac human ZO-1 (optimized for insect cell expression)	GenScript (Spadaro et al., 2017)	S1928
pSpCas9(BB)-2A-GFP (px458)	(Ran et al., 2013)	Addgene #48138
Software and Algorithms		
ImageJ	N/A	https://imagej.nih.gov/ij/
Photoshop	N/A	https://www.adobe.com
Adobe illustrator	N/A	https://www.adobe.com
SnapGene	N/A	http://www.snapgene.com/
Prism GraphPad	N/A	https://www.graphpad.com/scientific-software/prism/

CONTACT FOR REAGENT AND RESOURCE SHARING

Further information and requests for resources and reagents should be directed to and will be fulfilled by the Lead Contact, Sandra Citi (sandra.citi@unige.ch).

EXPERIMENTAL MODEL AND SUBJECT DETAILS

Mouse cortical collecting duct cells (mCCD clone N64-Tet-ON, a kind gift from Prof. Eric Feraille, University of Geneva, Switzerland) and human intestinal epithelial cell line (SKCO-15, a kind gift from Prof. Asma Nusrat, Emory University, Atlanta, USA) were grown in Dulbecco's modified Eagle's medium (DMEM, GIBCO) supplemented with 20% heat-inactivated fetal bovine serum (FBS; PAN Biotech), 1X minimal essential medium nonessential amino acids (MEM NEAA; GIBCO), 100U/ml of penicillin and 100U/ml of streptomycin. HEK293T cells were cultured in the same medium as above, supplemented with 10% FBS. Human Hap1 cells (WT, ADAM10-KO, PLEKHA7-KO, afadin-KO and Tspan33-KO) (Popov et al., 2015), human lung carcinoma cells (A427 and A549, a kind gift from Prof. Marco Paggi, Regina Elena National Cancer Institute, Rome, Italy), human colon carcinoma (SKCO), mouse cili-ated embryonic aorta-derived endothelial cells (meECs, a kind gift from Prof. Brenda Kwak, University of Geneva, Switzerland) and dog kidney proximal tubule cells (MDCK II Tet-off, a kind gift from Prof. Alan Fanning, University of North Carolina at Chapel Hill, NC, USA) were cultured as described previously (Popov et al., 2015, Vasileva et al., 2017). The sex of the lines was: MDCKII female, A427, A549, SK-CO-15 male. For other lines, sex was not listed in the information available to us. We trusted the providers of the cells for their authentication.

METHOD DETAILS

Genome Engineering

PLEKHA7-KO mCCD cells and PDZD11-KO Hap1 cells were generated using CRISPR/Cas9 gene editing technology. The guide RNA (gRNA) targeting the CRISPR sequence was identified and oligos corresponding to the gRNA was designed using the Zhang Lab CRISPR design tool (http://crispr.mit.edu/). Target sequences are described in Key Resources Table. Oligos were synthesized (Microsynth) and cloned into the BbsI site of Cas9 and GFP expressing px458 CRISPR plasmid (Addgene catalog no. 48138) as described in (Ran et al., 2013). WT mCCD cells or Hap1 cells were transfected (Lipofectamine2000) using px458 plasmid encoding gRNA for the target gene. At 48-hr post transfection, GFP positive cells were single-cell sorted into 96-well tissue culture plates containing preconditioned culture medium (using a Beckman Coulter MoFlo Astrios sorter at Flow cytometry service of University of Geneva Medical School). Single clones were further amplified and screened for knockout using immunoblot and immunofluorescence analysis. PLEKHA7-KO mCCD clones were further verified by Sanger sequencing. Genomic DNA was purified using the DNeasy®Blood and Tissue kit (QIAGEN catalog no. 69504), and for sequencing, the genomic locus of the control WT or PLEKHA7-KO clones was amplified by PCR (primers Forward CGTGTCAGGAAGGTGCATA, Reverse AGTGCCAGGACCACTC TGAC) and subcloned into pcDNA3.1(+) myc-His (EcoRI and HindIII). For genotyping the primers used are forward GTTTAACCA CACCGCTCCAG and reverse GCAGCTTACCGATTTTCCAT. PDZD11-KO mCCD cells and PLEKHA7-KO Hap1 cells were described previously (Guerrera et al., 2016; Popov et al., 2015). Afadin-KO Hap1 clones (Popov et al., 2015) was validated by immunoblot and immunofluorescence analysis. Tspan33-KO Hap1 clones (Popov et al., 2015) were validated by Sanger sequencing only, since no good commercial anti-Tspan33 antibody is available. Genomic locus was amplified by PCR (Forward TGGTGAGCC TAATGCCATTC and Reverse CAGGAAGAAGAGGCGTCTAG) followed by genotyping (sequencing primer, Forward TCCAACCA TAATGGAGATT).

Microarray analysis

Transcriptome profiling was performed with Affymetrix arrays containing 41,345 transcripts (iGE3 Genomics Platform-Bioinformatics). Total RNA was extracted from confluent WT and PLEKHA7-KO mCCD cells (clone-1) using NucleoSpin RNA II kit (Macherey-Nagel, catalog no. 740955.50). RNA quality was assessed by capillary electrophoresis on Agilent 2100 Bioanalyzer. 500 ng was amplified and labeled using the Ambion WT Expression kit (Affymetrix). Hybridization on GeneChip Mouse Gene 2.0 ST arrays (Affymetrix) was carried out according to the manufacturer's instructions. The data were robust multi array normalized (Bolstad et al., 2003). To assess the difference in gene-expression values between the PLEKHA7-KO and WT conditions, we applied a 1-way ANOVA with contrast in Partek Genomics Suite (http://www.partek.com). P values were corrected for multiple testing by use of the false-discovery rate (FDR) method of Benjamini and Hochberg (Hochberg and Benjamini, 1990). We applied a conservative significance threshold of 5% FDR associated with fold change value of 2 or more. Data were plotted in a scatterplot, which shows the average of the log normalized expression values of the PLEKHA7-KO samples as a function of the average of the log normalized expression values of the WT samples.

Antibodies and Plasmids

Antibodies are described in Key Resources Table. The anti-*S.aureus* α-toxin antibody (Sigma-Aldrich, catalog no. S7531) recognizes both monomeric and heptameric toxin. Constructs expressing YFP alone, YFP-PLEKHA7 and YFP-ΔWWΔPH PLEKHA7 were described in (Paschoud et al., 2014). Truncated PLEKHA7 constructs YFP-ΔWW (residues 90-1121) and YFP-ΔPH (residues 1-162 fused to 282-1121) was obtained by PCR and subcloning into NotI-ClaI sites of pTre2hyg vector. Constructs expressing CFP-HA, PDZD11-HA, GFP-PDZD11-myc and GFP-myc are described in (Guerrera et al., 2016). N-term PLEKHA7-myc (residues 1-500), WW (W1+W2)-PLEKHA7-myc (residues 1-162), and W2-PLEKHA7-myc (residues 50-163) was obtained by PCR and subcloned into BamHI-ClaI or BamHI-NotI sites of pTre2hyg. EGFP tagged TspanC8 plasmids i.e., human Tspan5, Tspan10, Tspan14, Tspan15, Tspan17 and Tspan33 were described in (Dornier et al., 2012). Synthetic cDNA coding for mouse Tspan15 and mouse Tspan33 (GeneScript) were PCR amplified and subcloned into HindIII-BamHI or NheI-AgeI sites of pEGFP-N3 respectively, with EGFP at the C terminus of the protein. C-terminal EGFP tagged mTspan15_mTspan33-C-term chimera was obtained by PCR amplification and subsequent restriction digestion of residues 1-257 of mTspan15 (HindIII-EcoRI) and residues 255-283 of mTspan33 (EcoRI-BamHI) and subcloned into HindIII-BamHI sites of pEGFP-N3. cDNA encoding human CD82 in pcDNA3 vector was PCR amplified and subcloned into EcoRI-AgeI sites of pEGFP-N1. Several C-terminal EGFP tagged hCD82-hTspan33 chimeras were generated by PCR amplifications and various fragments obtained were subcloned into the EcoRI-AgeI sites of pEGFP-N1 vector. For hTspan33, the LEL comprises amino acids 120-238 and the cytoplasmic C-terminal region comprises amino acids 262-283. For hCD82, LEL comprises amino acids 107-229 and cytoplasmic C-terminal region comprises amino acids 253-267. The chimeric Tspan33 molecule with its LEL region replaced with the LEL region of CD82 (Tspan33_CD82 –LEL) was obtained by PCR amplifications and subsequent restriction digestion of residues 1-119 (EcoRI-HindIII) and 239-283 (BamHI-AgeI) for Tspan33 and LEL region (HindIII-BamHI) of hCD82 and subcloned into pEGFP-N1 by three-way ligation. The chimeric CD82 molecule with its LEL region replaced with the LEL region of Tspan33 (CD82_Tspan33-LEL) was obtained by PCR amplifications and subsequent restriction digestion of residues 1-106 (EcoRI-HindIII) and 230-267 (BamHI-AgeI) for CD82 and LEL region (HindIII-BamHI) of Tspan33 and subcloned into pEGFP-N1. Finally the chimeric CD82 molecule with its both the LEL region and cytoplasmic C-term replaced by those of

Tspan33 was obtained by PCR amplification of CD82_Tspan33-LEL containing the whole fragment except the cytoplasmic C-term (EcoRI-XmaI) and cytoplasmic C-term of Tspan33 (XmaI-AgeI) and subcloned into pEGPF-N1. For GST pulldowns, GST tagged ADAM10 cytoplasmic C-term (residues 314-371, EcoRI-XhoI), Tspan33 N-term (residues 1-25, BamHI-NotI), Tspan33 C-term (residues 256-283, BamHI-NotI), PLEKHA7 N-term (residues 1-349, BamHI-XhoI) and nectin-1 C-term (residues 379-517, BamHI-XhoI) were generated by PCR amplification and subcloned into pGEX4T1 vector using the indicated restriction sites. Constructs expressing GST alone, GST-WW PLEKHA7, GST-PDZD11 and GST-C-term occludin were described previously (Guerrera et al., 2016, Cordenonsi et al., 1997). Various constructs coding for FLAG-tagged afadin (see also Key Resources Table) were a kind gift from Prof. Y. Takai (Kobe University, Japan) (Kurita et al., 2013).

Immunofluorescence, Immunohistochemistry and Proximity Ligation Assay
For immunofluorescence analysis (IF), cells were seeded onto 12-mm glass coverslips placed in 24 well plates (Falcon[TM] Polystyrene Microplates). For Hap1 cells, coverslips were precoated with 0.01% Poly-L-lysine (Sigma-Aldrich, catalog number P4707) for 15 min at 37°C prior to seeding. Conventional fixation of cells for labeling of junctional proteins was with methanol (10 min at $-20°C$) followed by incubation with primary antibodies (45 min at 30°C) and secondary antibodies (30 min at 37°C) diluted in PBS. To study the effect of confluency on ADAM10 localization, WT mCCD cells were seeded at density of 25'000 cells/coverslip (day 0) and fixed on day 2 (sparse), 4 (semi-confluent) and 6 (confluent) followed by IF. For IF analysis on polarized mCCD cells (to differentiate zonular apical versus lateral labeling of proteins), 1×10^5 mCCD cells were seeded onto 6.5 mm, 0.4-μm pore polycarbonate 24-well tissue culture inserts (Transwell filters; Corning Costar catalog no. 3470) and grown for 4-6 days, to achieve maximal polarization. To study the localization of exogenous GFP-Tspan15 and GFP-Tspan33, WT mCCD cells were transfected a day after seeding on the filters. Cells on filters were fixed using methanol ($-20°C$) overnight (15-18 hours) followed by 1-min treatment with acetone ($-20°C$). Filters were excised manually using a razor blade and hydrated in IF buffer (0.1% Triton X-100, 0.15 M NaCl, 5 mM EDTA, 20 mM HEPES, pH 7.5, 0.02% NaN$_3$ as preservative). Incubation with primary antibodies was overnight at 4° and with secondary antibodies for 3 hours at RT. The filters were placed on glass slides with the cells facing up and were mounted with a glass coverslip with Vectashield containing DAPI (Reactolab). To study the localization of α-toxin in mCCD cells grown on Transwell filters or in Hap1 cells grown on glass coverslips, cells were first intoxicated either for 1 hr (mCCD cells), or for 5 min or 30 min (Hap1 cells), followed by 3 washes with PBS, and methanol fixation and IF analysis as described above. Immunohistochemistry on mouse lung and kidney tissue sections was carried out as described previously (Pulimeno et al., 2010). Proximity Ligation Assay (PLA) (Sigma, catalog no. DU092101) was performed on WT and PDZD11-KO mCCD cells according to the manufacturer's instructions, using appropriate combinations of primary and secondary antibodies.

Cell transfections and siRNA-mediated depletion
All transfections were performed using Lipofectamine2000, following the manufacturer's guidelines (Invitrogen), 24 hr after plating 1×10^5 cells on either coverslips in 24-well plates or Transwell filters, and cells were analyzed by IF between 24 and 72 hr after transfection. The expression of constructs in the vector pTre2Hyg was carried out after selection in hygromycin (200 μg/ml), and induced by doxycycline (40 ng/ml) for at least 48 hours. The localization of GFP tagged tetraspanin proteins was determined using an anti-GFP antibody, except for live imaging. To study the localization of GFP-Tspan33 in sparse and confluent cells, 25'000 mCCD cells were seeded on glass coverslips (day 0) and transfected with GFP-Tspan33 the next day (day 1). GFP-TSPAN33 localization was analyzed 24 hr post transfection (Day 2, sparse) or 4 days post transfection (Day 6, confluent). For transient depletion using siRNA, cells were transfected using Lipofectamine RNAiMAX (Invitrogen) 24 hr post-seeding, according to the manufacturer's instructions. The siRNA used to target mouse *adam10* in mCCD cells are forward ATAAAGTACTTGATTATGA and reverse TCATAATCAAGTACT TTAT and the siRNA used to target mouse *plekha7* in mCCD cells are forward CTGATGACACCTACCTCCA and reverse TGGAGG TAGGTGTCATCAG. Cells were analyzed by immunoblotting or by immunofluorescence microscopy 48-72 hr post transfection. To study the localization of GFP-Tspan33 in the cells knockdown for PLEKHA7, siRNA against PLEKHA7 and GFP-Tspan33 plasmid were co-transfected (Lipofectamine2000) and cells were analyzed 48 hr post transfection.

Sample preparation, SDS-PAGE and Immunoblot analysis
SDS-PAGE and immunoblot analysis was carried out as described previously (Paschoud et al., 2014). Total cell lysates were prepared from confluent monolayer of cells grown in 6-well tissue culture plates using RIPA buffer (150 mM NaCl; 40 mM Tris-HCL, pH 7.5; 2 mM EDTA; 10% glycerol; 1% Triton X-100; 0.5% sodium deoxycholate; 0.2% SDS and protease inhibitor cocktail, Roche). To determine immature or mature levels of ADAM10 in the cells grown at different confluency, WT mCCD cells were seeded in 6- well plates at density 125'000 cells/well (day 0) and lysates were prepared on day 2, 4 and 6 post-seeding. Protein loadings were normalized by immunoblotting with anti-β-tubulin antibody. To detect α-toxin heptamers upon intoxication (also see methods section for "Intoxication"), the cell lysates were prepared as above, but the lysates were heated to 60°C for 5 min instead of 95°C for 5 min (adapted from (Cassidy and Harshman, 1979)).

Cell surface biotinylation
Cell surface biotinylation was performed using the Pierce[TM] Cell Surface Protein Isolation Kit following the manufacturer's guidelines (Thermo Fisher Scientific, catalog no. 89881). In brief, 90%–95% confluent WT or KO Hap1 cells seeded in P60 plates were treated

with α-toxin (20U/ ml) for 30 min. Non-treated cells were used as negative control. Following the treatment, the cells were washed with Hap1 medium and allowed to recover in fresh medium for 6 hr. The surface proteins were labeled with EZ-Link[TM] Sulfo-NHS-SS-Biotin dissolved in PBS for 30 min at 4°C. After quenching the reaction using quenching solution and multiple washes with TBS (3X), the cells were lysed (lysis buffer provided in the kit) and the biotinylated proteins were isolated by incubating the lysates overnight at 4°C (with rotation) with 50 μL of NeutrAvidin agarose. A small fraction of the lysate was kept aside (total lysate). After multiple washes with wash buffer, the bound proteins are released by incubating with SDS-PAGE sample buffer (containing 50 mM DDT) for 30 min at RT and followed by heating at 65°C for 5 min. 10 μL of the eluate along with 1/10th amount of total cell lysate was analyzed for α-toxin heptamers by SDS-PAGE and immunoblotting.

Co-Immunoprecipitation assay

Co-immunoprecipitation assay was performed as described in (Guerrera et al., 2016). Briefly, Hap1 cells (or Hap1 cells transfected with GFP-Tspan33) were lysed in Co-IP buffer (150 mM NaCl, 20 mM Tris-HCl, pH 7.5, 1% Nonidet P-40, 1 mM EDTA, 5 mg/ml anti-pain, 5 mg/ml leupeptin, 5 mg/ml pepstatin, 1 mM PMSF). Dynabeads protein G (or protein-A when guinea pig anti-PLEKHA7 was used) (Invitrogen) was coupled to antibodies (2 μL of either pre-immune serum or 2 μL immune serum) for 90 min. Following multiple washes, the beads were incubated overnight with cell lysates (50 to 100 μL volume, previously normalized using β-tubulin or exogenous GFP-Tspan33). After multiple washes with Co-IP buffer, the immunoprecipitates were eluted from beads in 20 μL SDS sample buffer, boiled for 5 min at 95°C, and analyzed by SDS-PAGE and immunoblotting (10 μL of eluate was loaded along with 1/10 of the total cell lysate as the input).

GST pulldowns

For the production and purification of GST fusion protein baits, *E. coli* (BL21-DE3) transformed with constructs in pGEX4T1 were induced with 0.1 mM IPTG for 2 h at 37°C. Bacterial pellets were lysed using lysis buffer (PBS containing 1% Triton X-100, 5 mg/ml antipain, 5 mg/ml leupeptin, 5 mg/ml pepstatin, 1 mM PMSF) and cell debris removed by centrifugation at 13,000 g for 15 min at 4°C. The supernatants containing soluble GST tagged proteins were normalized for protein content by SDS-PAGE.

Prey proteins, were expressed in HEK293T (HEK) cells (2x10^{6} cells plated in 100 mm[2] dish) by transfecting with 20 μg of either HA-tagged or GFP-tagged constructs), lysed in Co-IP buffer, 48 hr after transfection. ZO-1 (Cordenonsi et al., 1999) or afadin were expressed in baculovirus infected insect cells (Sf9) and subsequently lysed in Co-IP buffer. Protein loadings of prey were normalized by immunoblotting. For GST pulldowns 2-5 μg of bait GST fusion protein was coupled for 1 hr at room temperature to 15 μL of glutathione-Sepharose beads. Following incubation and 3X washing with PBS containing 2% BSA and 1% NP-40, the beads were incubated for 2 hr at 4°C with normalized lysates of either HEK cells or insect cells. Proteins bound to the beads were eluted with 20 μL of SDS sample buffer at 95°C for 5 min, and 10 μL of eluate was loaded on SDS gels. Since lysates were used as preys, and not purified proteins, it cannot be formally excluded that contaminating proteins from the prey lysates may affect the results; however, it is unlikely that they are present in sufficiently high concentrations in lysates from cells (where the prey was overexpressed), to affect results.

Intoxication, cell viability assay and flow cytometry

Cells were intoxicated with α-toxin (Sigma-Aldrich, catalog no. H9395), except in the case of experiments using Alexa647 tagged α-toxin. Different toxin batches were titrated with Hap1 WT cells to obtain approximately 80% cell death after 24 hr treatment, and the number of units was adjusted to obtain approximately similar specific activity. To study the effect of confluency on α-toxin induced cell death, 1x10^{5} WT mCCD cells were seeded on Transwell filters (day 0) and intoxicated basolaterally using 100 U/ml of α-toxin for 8 hr on day 2, 4 and 6 post seeding. Following trypsinization, the cells were labeled using propidium iodide (PI, 2 μg/ml) for 30 min on ice and cell viability was determined using flow cytometry (BD Accuri C6 Plus, FACS analyzer). To study the effect of intoxication on WT, PLEKHA7-KO and PDZD11-KO mCCD cells, the cells were intoxicated on day 4 post-seeding by administering 100U/ml of α-toxin basolaterally for 24 hr at 37°C. Cell viability was determined by PI staining and FACS cytometry. Hap1 cells (genotypes as mentioned in the figures) were seeded at 2x10^{5} cells per well in 24-well plates a day before intoxication and then treated with 20U/ml (if otherwise stated) of α-toxin for 24 hr at 37°C followed by trypsinization, PI staining and FACS analysis. Intracellular ATP levels was assessed at different times (15', 30', 1 hr, 2 hr, 3 hr, 4 hr, 8 hr or 24 hr) post-intoxication (with increasing toxin doses, as indicated) of Hap1 cells using CellTiter-Glo Luminescent cell viability assay kit (Promega, catalog no. G7570) and read using a microplate reader (Cytation 3, BioTek) as described previously (Popov et al., 2015). For PLEKHA7-KO Hap1 cells, the percentage of cell death after 24 hr treatment varied between 10% and 40%, depending on toxin batch.

Pharmacological inhibition of cellular processes

Amiloride (50 μM in DMSO, Sigma-Aldrich catalog no. A3085) and Wortmannin (400 ng/ml in DMSO, Cell Signaling Technology, catalog no. 9951S) were used to inhibit macropinocytosis while Latrunculin-A (Lat-A) (200 nM in DMSO, Sigma-Aldrich catalog no. L5163) was used to prevent actin polymerization in Hap1 cells. The final concentrations of inhibitors were determined on the basis of dose-response curves (not shown). Hap1 cells (2x10^{5}, genotype as indicated in the figure panels) were seeded a day before the experiment. The cells were pretreated for 1 hr with the inhibitor followed by α-toxin treatment (20U/ ml) in presence of the inhibitor for 6 hr (amiloride, since it was toxic when treated for longer than 6 hr) or 24 hr (Wortmannin) at 37°C. In case of Lat-A, the pre-treatment

was for 2 hr, followed by α-toxin treatment (10U, 20U or 40U/ ml) in the presence of inhibitor for 1 hr. Both the toxin and Lat-A was then removed by multiple washes with medium and then the cells were allowed to recover in fresh medium for 24 hr at 37°C. Lat-A treatment for more than 3-4 hr was toxic to Hap1 cells. Cells treated with DMSO only or inhibitor only or α-toxin only were used as controls. Cell viability was determined by PI staining and FACS cytometry as described before.

Confocal microscopy and live-cell imaging

Imaging of fluorescently labeled methanol fixed samples was performed using a Zeiss LSM700 confocal microscope, equipped with a 63X, 1.3NA oil objective. For live-cell imaging, Hap1 cells, either in the presence or the absence of transiently transfected GFP-Tspan33, was incubated with 500 ng/ml of Alexa647 tagged α-toxin (Virreira Winter et al., 2016) (a kind gift from Prof. A. Zychlinsky, Max Planck Institute, Berlin, Germany), for the indicated time in live imaging solution (Thermo Fisher Scientific, catalog no. A14291DJ) supplemented with 10% FBS and mounted on a temperature controlled stage (37°C). Live cell imaging was performed using a confocal Leica-SP8 inverted microscope, using a 63X, 1.3NA oil objective.

QUANTIFICATION AND STATISTICAL ANALYSIS

Data processing and analysis was performed using GraphPad Prism7. All experiments were performed at least three independent times and one representative image is shown. For statistical analysis of quantifications, unpaired two-tailed Students t test or one-way ANOVA were used (*p < 0.5, **p < 0.01, ***p < 0.001).

Analysis of immunofluorescence (IF) signals:

The junctional / cell contact IF signal was quantified by measuring the pixel intensity of the selected junctional area using polyhedral tool of ImageJ for a) the protein of interest and b) the internal junctional reference standard (either PLEKHA7 or ZO-1). The average background pixel intensity was subtracted from the junctional pixel intensity for each channel. Relative signal was expressed as the ratio between pixel intensity of the protein of interest to the pixel intensity of the reference protein. The data is represented as boxplot with the median and hinges corresponding to the 25th and 75th percentiles, and the whiskers corresponds to the minimum and maximum of the data (Figure 1E (top), n = 10-15; Figure 6B, n = 26; Figure S4J, n = 50). Quantification of toxin accumulation at the cell-cell contacts of Hap1 cells was carried out as described above but the data are represented as mean with standard deviations for each time point (Figure S5C, n = 10). The cytoplasmic ADAM10 signal was quantified by measuring the pixel intensity of the cytoplasm (selected as the region inside the cells excluding cell-cell junctions) and represented as boxplot (Figure 1E (bottom), n = 10-16). To analyze cytoplasmic versus junctional ADAM10 or Tspan33 signal, ratio between the pixel intensity of the cytoplasm to the pixel intensity of junctional area (selected using polyhedral tool of ImageJ using ZO-1 or PLEKHA7 as the junctional marker) of the same cell was calculated and represented as box-plot (Figure 2F, n = 10-15 Figure S4D, n = 15) or composite histogram showing percentage of cytoplasmic and junctional Tspan33 (Figure 5B, n = 14). The length of cell-cell contacts of WT or afadin-KO Hap1 cells was determined by measuring the distance between the ends of the cell-cell contacts using segmented line option in ImageJ and represented as boxplot as mentioned above (Figure S6D, n = 30-40).

Analysis of immunoblotting data

Quantification of mature versus immature levels of ADAM10 was obtained by densitometric analysis using ImageJ. Each histogram represents the mean (with standard deviations) of 3-densitometric analysis carried out on 3 independent experimental repeats (Figure 1G, Figure S4G, n = 3). To quantify levels of α-toxin pores in mCCD cells, densitometric analysis was carried out on immunoblot, and the signal was normalized to the levels of β-tubulin (Figure 6C, n = 3). For quantification of IP experiments, the pre-immune control signal was subtracted from the immunoprecipitate signal and normalized to the input signal (i.e., input GFP-Tspan33) from WT or PDZD11-KO Hap1 cell lysates (Figure S7D, n = 3).

PLA signal quantifications

The average number of dots (signal) per cell was calculated using ImageJ. The data is represented as boxplots as described before (Figure S7A, n = 50; Figures S7B and C, n = 20-30).

Cell-death analysis

Analysis of cell death was performed using Flow cytometry by calculating the percentage of cells positive for propidium iodide (10'000 cells analyzed for each sample). The data are represented as the mean of 3 measurements, and plotted as histograms (Figures 1H, 3D, 6J, 6G, and 6H, and Figures S3D, S5G, and S6F).

Supplemental Information

A Dock-and-Lock Mechanism Clusters ADAM10

at Cell-Cell Junctions to Promote

α-Toxin Cytotoxicity

Jimit Shah, Florian Rouaud, Diego Guerrera, Ekaterina Vasileva, Lauren M. Popov, William L. Kelley, Eric Rubinstein, Jan E. Carette, Manuel R. Amieva, and Sandra Citi

Figure S1. Antibody validation and localization and expression of ADAM10 in different cell types. Related to Figure 1.

(A-D) Validation of rabbit anti-ADAM10 antibody by IF (A, C) and IB analysis (B, D) either in mCCD cells depleted of ADAM10 by siRNA (A-B) or Hap1 cells KO for ADAM10 (C-D) (im=immature ADAM10, ~90 kDa, m= mature ADAM10, ~68 kDa). PLEKHA7 and ZO-1 are used as markers of zonular apical junctions in mCCD cells (A), and of adherens junctions (AJ) in Hap1 cells (C). Asterisks mark the cells depleted of ADAM10 (A). Arrows indicate co-localization at junctions, white arrowheads indicate reduced/undetected junctional localization and yellow arrowheads indicate cytoplasmic/non-junctional labeling.

(E-F) Immunofluorescent localization (E) or immunoblot analysis (F) of ADAM10 in different cell types, as indicated in the figure panels. *Zonula adhaerens* markers (PLEKHA7 or p120-ctn) or the TJ marker (ZO-1) are used to label cell-cell junctions in (E). Bar =20 μm.

Figure S2. Characterization of PLEKHA7-KO mCCD cells, and localization of ADAM10 in PLEKHA7- KO mCCD and Hap1 cells. Related to Figure 2.

(A-C) Characterization of PLEKHA7-KO mCCD clonal lines (1, 5 and 7) by sequencing (A), IF (B) and IB analysis (C). The CRISPR target sequence for the gRNA is indicated with red text within the red box. Insertions and/or deletions are indicated for both alleles for each of the 3 PLEKHA7-KO clonal lines, below the WT sequence.

(D, E, G) IF localization of ADAM10 in either WT or PLEKHA7-KO mCCD cells (clones 5 and 7) (D), or mCCD cells depleted of PLEKHA7 by siRNA (depleted cells indicated by asterisks in E) or in either WT or PLEKHA7-KO Hap1 cells (G). PLEKHA7, E-cadherin and ZO-1 are used as junctional markers in mCCD cells (B, D, E, I) and Hap1 cells (G) (E-cadherin: zonular+lateral in mCCD cells; PLEKHA7 and ZO-1: zonular in mCCD cells and junctional in Hap1 cells).

(F-H) Immunoblotting analysis of ADAM10 either in cells depleted of PLEKHA7 by siRNA (F) or in Hap1 WT and KO cells (H). See Figure 2 for labeling.

(I) IF localization of YFP-tagged WW-PLEKHA7 in WT mCCD cells. Bars= 20 μm.

Figure S3. Localization of ADAM10 in PDZD11-KO cells, and kinetics of intracellular ATP loss in WT and KO lines upon toxin treatment. Related to Figure 3.

(A-B) Characterization of PDZD11-KO Hap1 cells either by immunoblot (A) or IF (B), using anti-PDZD11 antibodies (Guerrera et al., 2016).

(C) IF localization of ADAM10 either in WT (top) or PDZD11-KO (bottom) Hap1 cells. Bars= 20 μm.

(D) Percentages of cell death (propidium iodide staining) either in control WT/KO cells or in WT/KO cells treated with α-toxin. Asterisks indicate statistical significance.

(E-H) Measurement of total intracellular ATP levels upon treatment of Hap1 cells (genotypes as labeled in the graph - panel H) using different concentrations of α-toxin (10 U/ml, E; 20 U/ml, F; 30 U/ml, G and 50 U/ml, H) and at different time points as indicated in the X-axis.

A

PLEKHA7-KO cells (y-axis) vs WT cells (x-axis)

Tspan15, Tspan14, Tspan5, Tspan33, Tspan17, Tspan10

B

GFP (Tspan5) | GFP(Tspan10) | GFP (Tspan14) | GFP (Tspan15) | GFP (Tspan17) | GFP (Tspan33)

C

sparse: GFP (Tspan33) | ZO-1 | MERGE

confluent: GFP (Tspan33) | ZO-1 | MERGE

mCCD-coverslips

D

cytopl. / junct. Tsp33

Sparse, Confluent

***

E

human Tspan33

PAM (CRISPR/Cas9 target guide site)

WT .....CTGTGGCTGCATTGGGTCCCTCCGCGAGAACATCTGCCTCCTGCAGACGGTGAGTGGTCA.....

Tspan33-KO .....CTGTGGCTGCATTGGGTCC------------------------TGCCTCCTGCAGACGGTGAGTGGTCA.....
2.3   (18 bp deletion)

Tspan33-KO .....CACCTTCTGTGGCTGCATT............GCGAGAACATCTGCCTCCTGCAGACGGTGAGTGGTCA.....
2.5   (10 bp deletion and 151 bp insertion)

Tspan33-KO .....CTGTGGCTGCATTGGGTCCCTCCAGCGAGAACATCTGCCTCCTGCAGACGGTGAGTGGTCA...
2.8   (1 bp insertion)

F

kDa | WT | KO 2.3 | KO 2.5 | KO 2.8
100 / 75: im, m ← IB:AD-10
50: IB:β-Tubulin

Hap1 cells

G

m/im ADAM10

WT, KO 2.3, KO 2.5, KO 2.8

ns

H

WT: ADAM 10 | PLEKHA7 | MERGE | ZO-1

Tspan33-KO: ADAM 10 | PLEKHA7 | MERGE | ZO-1

Hap1-coverslips

I

WT: ADAM10 | GFP (Tspan33) | MERGE | PLEKHA7

mCCD-covers.

J

Ratio (AD10/P7)

Tspan33 +, −

***

K

WT: ADAM10 | GFP (Tspan33) | MERGE | PLEKHA7

Hap1-covers.

L

GFP | PLEKHA7 | MERGE

GFP-T15_33Cterm CHIMERA | PLEKHA7 | MERGE

mCCD-coverslips

Tspan15:
Tspan33-Cterm

M

si-control: GFP (Tspan33) | PLEKHA7 | MERGE | ZO-1

siPLEKHA7: GFP (Tspan33) | PLEKHA7 | MERGE | ZO-1

mCCD-coverslips

Figure S4. Expression and localization of TspanC8s, characterization of Tspan33-KO Hap1 cells, and role of Tspan33 in ADAM10 localization. Related to Figure 4 and Figure 5.

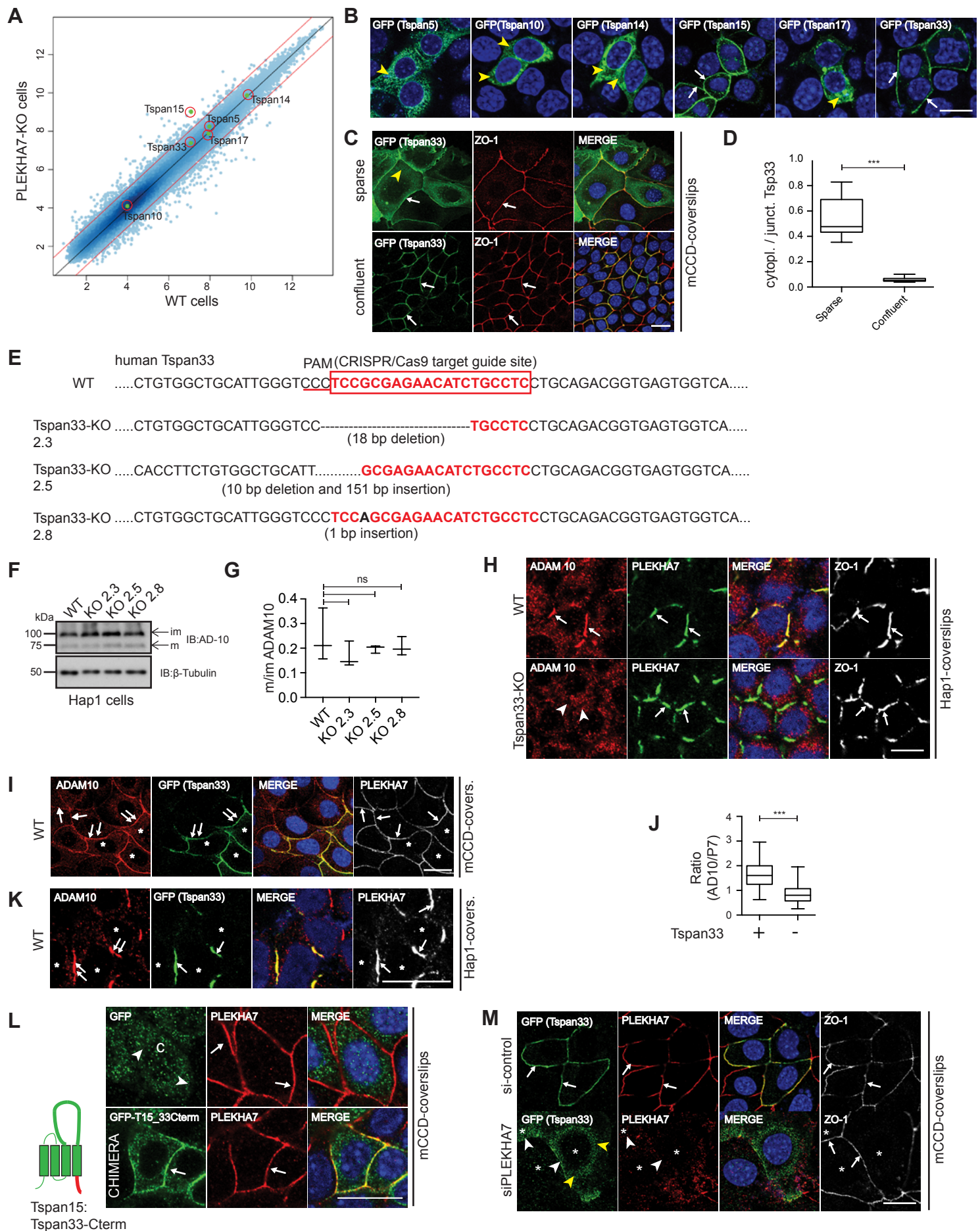(A) Differential gene expression profile of PLEKHA7-KO vs WT mCCD cells. Each dot represents an Affymetrix transcript_cluster_id, and the red lines represent the fold change threshold of 2. Probes for TSPAN5, TSPAN10, TSPAN14, TSPAN15, TSPAN17 and TSPAN33 are indicated by red circles.

(B) IF localization of GFP-tagged TspanC8 proteins in WT mCCD cells. White arrows indicate localization at cell surface/junctions. Yellow arrowheads indicate cytoplasmic localization. Only Tspan15 and Tspan33 are localized predominantly at the cell surface/junctions.

(C-D) IF localization of GFP-Tspan33 in either sparse (top) or confluent (bottom) WT mCCD cells (C), and quantification of cytoplasmic versus junctional GFP-Tspan33 (D). Tspan33 accumulation at junctions increases in confluent cells.

(E) Sequence validation of Tspan33-KO Hap1 clonal lines (2.3, 2.5 and 2.8) (Popov et al., 2015). The target guide sequence (red box) in WT, and insertions/deletions in the KO clones are indicated.

(F-H) IB analysis (F), densitometric quantification (G) and IF localization (H) of ADAM10 in Tspan33-KO Hap1 cells. White arrowheads indicate lack of junctional ADAM10 labeling in Tspan33-KO cells.

(I-J) IF localization of ADAM10 in WT mCCD cells, after transient transfection with GFP-Tspan33 (I) and quantification (J) of junctional ADAM10 ratioed to PLEKHA7. Double arrows indicate junctions of cells expressing GFP-Tspan33. Asterisks indicate either cells positive for transfection (I) or statistical significance (D, J).

(K) IF co-localization of exogenous GFP-Tspan33 with endogenous ADAM10 at junctions of WT Hap1 cells. Double arrows indicate increased ADAM10 labeling in cells overexpressing Tspan33 (indicated by asterisks).

(L) IF localization of Tspan15-Tspan33 chimera in WT mCCD cells and scheme of chimera on bottom left. Arrows idicate junctional localization of chimera.

(M) IF localization of exogenous GFP-Tspan33 in WT mCCD cells either treated with control siRNA (top) or with PLEKHA7 siRNA (bottom). Arrows indicate Tspan33 labeling colocalized at junctions with PLEKHA7 and ZO-1, white and yellow arrowheads indicate lack of Tspan33 junctional labeling and cytoplasmic labeling, respectively. Bars= 20 μm.

A

WT control — α-toxin / PLEKHA7 / MERGE

WT + toxin — α-toxin / PLEKHA7 / MERGE

Adam10-KO + toxin — α-toxin / PLEKHA7 / MERGE

Hap1 coverslips

B

Hap1 cells

control — WT / AD10-KO   treated — WT / AD-KO

150 — IB: α-toxin heptamer

50 — IB: β-Tubulin

C

- Wild-type
- PLEKHA7-KO
- PDZD11-KO

Ratio (α-toxin / ZO-1) at cell-cell contacts

Control, 5-mins, 30-mins, (R) 2 hrs, (R) 4 hrs

D

Wild-type / PLEKHA7-KO / PDZD11-KO

alexa-647 α-toxin

0 mins

+ Alexa647 α-toxin: 30 mins, 60 mins

Hap1 - plates live imaging

E

alexa-647 α-toxin / GFP-Tspan33 / MERGE

WT

ADAM10-KO

PLEKHA7-KO

PDZD11-KO

Hap1 plates live imaging

F

WT — control: anti-α-toxin (no toxin) / PLEKHA7 / MERGE / ZO-1

WT — + α-toxin: anti-α-toxin / PLEKHA7 / MERGE / ZO-1

Tspan33-KO — control: anti-α-toxin (no toxin) / PLEKHA7 / MERGE / ZO-1

Tspan33-KO — + α-toxin: anti-α-toxin / PLEKHA7 / MERGE / ZO-1

Hap1-coverslips

G

Hap1 cells

cell-death (%)

- control
- Treatment

WT, AD10-KO, Tsp33-KO-2.3, Tsp33-KO-2.5, Tsp33-KO-2.8

*** *** *** ***

Figure S5. Validation of α-toxin antibody, live imaging of α-toxin and GFP-Tspan33 in WT and KO cell lines, and role of Tspan33 in junctional toxin clustering. Related to Figure 6.

(A-B) IF (A) and IB analysis (B) of either WT or ADAM10-KO Hap1 cells treated with α-toxin. Untreated cells are used as controls. α-toxin IF labeling (A) and α-toxin heptamers (B) are detected in α-toxin-treated WT, but not ADAM10-KO Hap1 cells.

(C) Quantification of α-toxin labeling at cell-cell contacts related to Figure 6D-F, expressed as a ratio between α-toxin and ZO-1 labeling.

(D) Snapshots from live cell imaging of either untreated Hap1 cells (0 min) or cells treated for the indicated time with Alexa647-tagged α-t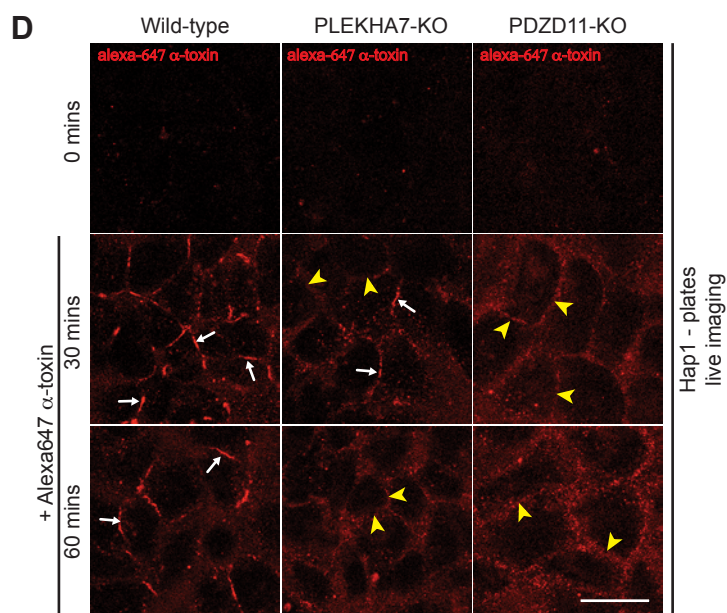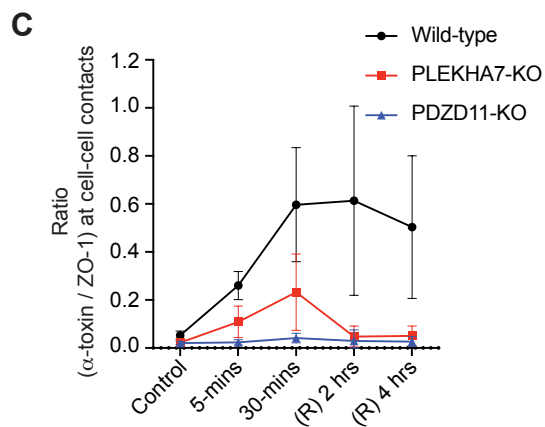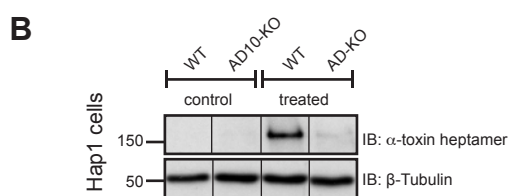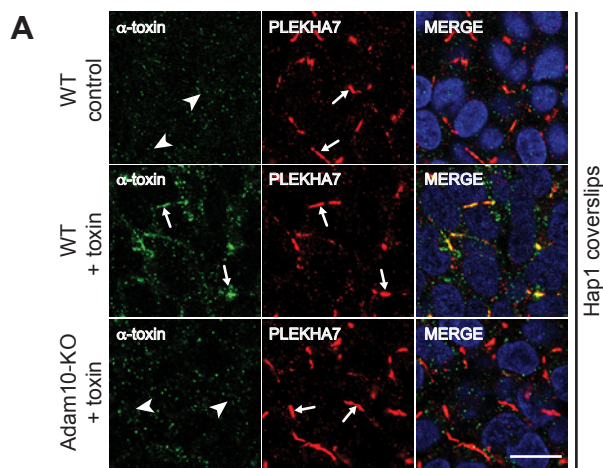oxin (Winter et al., 2016). α-toxin labeling is strong (arrows) and stable in WT cells, but weak (arrows) and/or undetected (yellow arrowheads) in PLEKHA7-KO and PDZD11-KO cells.

(E) Snapshots from live cell imaging of either WT, or ADAM10-KO, or PLEKHA7-KO or PDZD11-KO Hap1 cells expressing GFP-Tspan33 and treated for 30 min with Alexa647-tagged α-toxin. Yellow arrowheads indicate surface labeling by GFP-Tspan33, which is occasionally overlapped with toxin labeling. Tspan33 labeling clusters at junctions in WT and ADAM10-KO cells, but is distributed all over the cell surface in PLEKHA7-KO and PDZD11-KO cells (yellow arrowheads). α-toxin is clustered at junctions only in WT cells (white arrows).

(F) IF localization of α-toxin in either WT (upper panels) or Tspan33-KO Hap1 cells (bottom panels). Clustered toxin labeling is abolisged in Tspan33-KO cells (white arrowheads), despite the presence of PLEKHA7 (arrows). Bars= 20 μm.

(G) Percentages of cell death either in WT Hap1 cells, or in cells KO for either ADAM10 or Tspan33 (3 clonal lines) either untreated, or treated with α-toxin. Asterisks indicate statistical significance. KO of Tspan33 protects cells from death by α-toxin.

Figure S6. The role of afadin in the junctional clustering of PLEKHA7, ADAM10, Tspan33 and α-toxin in Hap1 cells. Related to Figure 7.

(A-B) Validation of afadin-KO Hap1 cells by IF localization (A) of afadin, PLEKHA7 and ZO-1 either in WT (upper panels) or in afadin-KO (bottom panels) Hap1 cells, and by IB analysis of afadin in WT and KO Hap1 cell lysates (B).

(C-D) IF localization of ADAM10 (C) and quantification of length of cell-cell contacts (D) either in WT (top, C) or Afadin-KO (bottom, C) Hap1 cells. ADAM10 clustered localization is reduced/undetected (red arrow) in junctions of afadin-KO cells. PLEKHA7 localization is either reduced/undetected (red arrow) or rarely detected (white arrow) in ZO-1 containing junctions of afadin-KO Hap1 cells.

(E) IF localization of α-toxin either in WT (top) or afadin-KO (bottom, higher magnification of boxed region in 6X zoom panels) Hap1 cells. Red arrowheads/arrows indicate reduced/undetected toxin and PLEKHA7-labeling in junctions that are labelled for ZO-1- White arrowhead in 6x toom panel indicates lack of ZO-1 labeling at sites labelled for α-toxin (hence containing ADAM10) and PLEKHA7 (arrows).

(F) Percentages of cell death (PI staining) upon treatment of either WT, PLEKHA7-KO or afadin-KO cells with α-toxin. Asterisks indicate statistical significance.

(G) IF localization of exogenous GFP-Tspan33 and α-toxin in either WT or afadin-KO Hap1 cells. Both Tspan33 and PLEKHA7 clustered labeling are disrupted following Tspan33 KO.

A

PLEKHA7::ADAM10 (signal/cell)
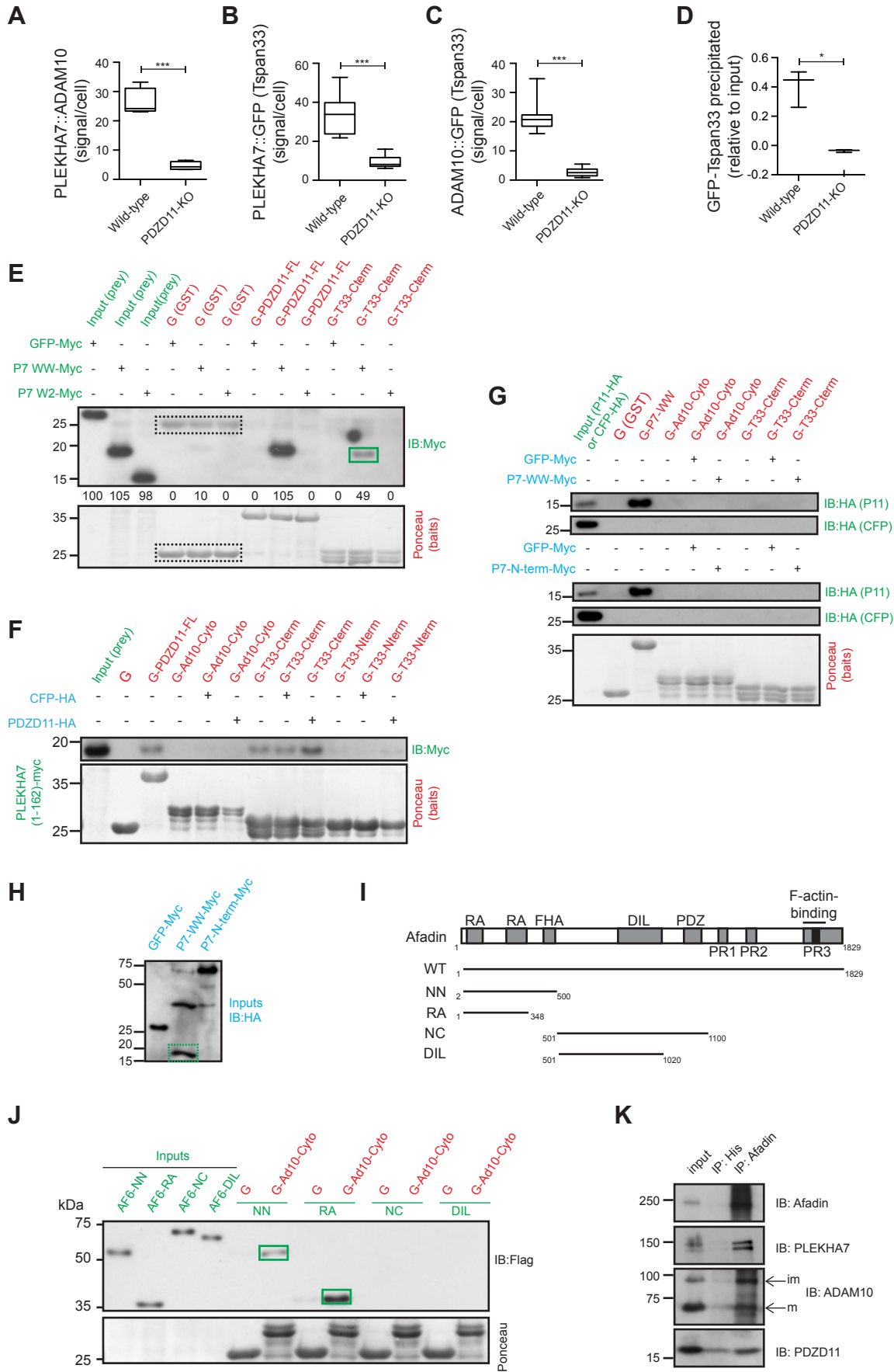
Wild-type, PDZD11-KO

***

B

PLEKHA7::GFP (Tspan33) (signal/cell)

Wild-type, PDZD11-KO

***

C

ADAM10::GFP (Tspan33) (signal/cell)

Wild-type, PDZD11-KO

***

D

GFP-Tspan33 precipitated (relative to input)

Wild-type, PDZD11-KO

*

E

Input (prey), Input (prey), Input (prey), G (GST), G (GST), G (GST), G-PDZD11-FL, G-PDZD11-FL, G-PDZD11-FL, G-T33-Cterm, G-T33-Cterm, G-T33-Cterm

GFP-Myc: + − − + − − + − − + − −
P7 WW-Myc: − + − − + − − + − − + −
P7 W2-Myc: − − + − − + − − + − − +

IB:Myc

25 / 20 / 15

100 105 98 0 10 0 0 105 0 0 49 0

Ponceau (baits)

35 / 25

F

Input (prey), G, G-PDZD11-FL, G-Ad10-Cyto, G-Ad10-Cyto, G-Ad10-Cyto, G-T33-Cterm, G-T33-Cterm, G-T33-Cterm, G-T33-Nterm, G-T33-Nterm, G-T33-Nterm

CFP-HA: − − − − + − − + − − + −
PDZD11-HA: − − − − − + − − + − − +

IB:Myc

20

PLEKHA7 (1-162)-myc

Ponceau (baits)

35 / 25

G

Input (P11-HA or CFP-HA), G (GST), G-P7-WW, G-Ad10-Cyto, G-Ad10-Cyto, G-Ad10-Cyto, G-T33-Cterm, G-T33-Cterm, G-T33-Cterm

GFP-Myc: − − − + − − + −
P7-WW-Myc: − − − − + − − +

IB:HA (P11)   15
IB:HA (CFP)   25

GFP-Myc: − − − + − − + −
P7-N-term-Myc: − − − − + − − +

IB:HA (P11)   15
IB:HA (CFP)   25

Ponceau (baits)   35 / 25

H

GFP-Myc, P7-WW-Myc, P7-N-term-Myc

75 / 50 / 25 / 20 / 15

Inputs IB:HA

I

F-actin-binding

Afadin: RA RA FHA DIL PDZ PR1 PR2 PR3
1 ──────────────────────── 1829

WT 1 ──────────────────────── 1829
NN 2 ──── 500
RA 1 ─── 348
NC 501 ──────── 1100
DIL 501 ───── 1020

J

Inputs: AF6-NN, AF6-RA, AF6-NC, AF6-DIL | G, G-Ad10-Cyto (NN), G, G-Ad10-Cyto (RA), G, G-Ad10-Cyto (NC), G, G-Ad10-Cyto (DIL)

kDa   75 / 50 / 35 / 25

IB:Flag

Ponceau   25

K

input, IP : His, IP : Afadin

250   IB: Afadin
150   IB: PLEKHA7
100 / 75   IB: ADAM10   im / m
15   IB: PDZD11

Figure S7. Tspan33 binds to the WW domains of PLEKHA7, but not either to the W2 domain of PLEKHA7 or to PDZD11. Related to Figure 7.

(A-C) Box-plots showing quantification of the junctional PLA signal (average dots/cell) obtained from (Figure 7B-D) respectively. PLA signal corresponding to the complex between PLEKHA7, ADAM10 and Tspan33 decreases dramatically upon KO of PDZD11.

(D) Histograms, showing the quantification of IB signals for IPs shown in (Figure 7F). Complex formation between PLEKHA7 and Tspan33 is dramatically reduced upon KO of PDZD11.

(E) The C-term of Tspan33 binds to the WW (W1+W2) but not the W2 domain of PLEKHA7. IB analysis, using anti-myc antibodies, of GST pulldowns using either GST (negative control=G), GST-PDZD11 (full length, positive control) or GST fused to the cytoplasmic C-terminal region of tetraspanin33 (G-T33-Cterm) as baits, and either GFP-myc (negative control) or myc-tagged WW region of PLEKHA7 (=P7 WW-Myc, 1-162) or myc-tagged W2 region of PLEKHA7 (=P7 W2-Myc, 50-162) as preys.

(F) The C-term, but not the N-term of Tspan33 binds to the WW domain of PLEKHA7, and the interaction is enhanced by PDZD11. IB analysis, using anti-myc antibodies, of GST pulldowns using either GST, or GST-PDZD11 (full length, positive control) or GST fused to the cytoplasmic C-terminal region of ADAM10, or the cytoplasmic C-terminal region of tetraspanin33 (G-T33-Cterm), or the cytoplasmic N-terminal region of tetraspanin33 (G-T33-Nterm) as baits, and the myc-tagged WW region of PLEKHA7 (PLEKHA7 1-162) as prey, in the presence of either CFP-HA (negative control) of PDZD11-HA (third molecule).

(G-H) PDZD11 does not bind to either the C-term of ADAM10 orTspan33, regardless of the presence of WW domain of PLEKHA7. (G) IB analysis, using antibodies against HA, of GST pulldowns using either GST (negative control) or GST tagged to cytoplasmic C-terminal region of ADAM10 (=G-Ad10-Cyto) or GST tagged to cytoplasmic C-terminal region of Tspan33 (=G-T33-Cterm) as baits, and either CFP-HA (negative control) or PDZD11-HA (P11-HA) as preys. Pulldowns were carried out in the presence of additional ligands. Top: either GFP-myc (negative control) or WW regions of PLEKHA7 tagged with myc (P7-WW-Myc). Bottom: either GFP-myc (negative control) or the N-terminal region of PLEKHA7 tagged with Myc (=P7-N-term-Myc, 1-500). (H) Normalization of third molecules, GFP-Myc, PLEKHA7-WW-Myc and PLEKHA7-N-terminal-Myc.

(I-J) The RA domain of afadin binds to the C-terminal domain of ADAM10. Schematic diagram of afadin, with indicated structural domains (Kurita et al., 2013), FLAG-tagged constructs used as baits for GST pulldowns (I), and IB analysis of pulldowns (J) using either GST (G) or GST fused to the C-terminal region of ADAM10 as baits. Ponceau-S-stained blots show the amounts of recombinant proteins used as bait. Numbers below the blots indicate quantification of preys by densitometry. Baits are marked in red, primary inputs in green and secondary inputs in blue.

(K) Afadin forms a complex with PLEKHA7, ADAM10 and PDZD11. IB analysis of IPs obtained either with rabbit anti-His serum (negative control) or rabbit anti-afadin, and immunoblotted either with antibodies against afadin or PLEKHA7, or ADAM10 or PDZD11. Lysates for IPs were prepared from WT Hap1 cells.